MEMORY AND BISTABILITY IN THE PHEROMONE RESPONSE PATHWAY

Lior Vered

A dissertation submitted to the faculty at the University of North Carolina at Chapel Hill in partial fulfillment of the requirements for the degree of Doctor of Philosophy in the Department of Chemistry (Molecular and Cellular Biophysics).

Chapel Hill
2018

Approved by:

Henrik Dohlman

Timothy Elston

Beverly Errede

Dorothy Erie

Nancy Thompson

ABSTRACT

Lior Vered: Memory and Bistability in The Pheromone Response Pathway
(Under the direction of Timothy Elston and Beverly Errede)

Polarity is the asymmetric organization of cellular structures, and is critical for differentiation, morphogenesis and migration in all eukaryotes. Many mathematical models of polarity rely on the existence of two stable steady states, and which state is observed depends on past conditions. However, bistable regulation of polarity has yet to be proven experimentally.

One of the hallmarks of a bistability is hysteresis, a mechanism of memory in which the response of a system depends on its history. To identify hysteresis, we compared the minimum pheromone concentration needed to establish polarity with the minimum concentration needed to maintain polarity. Using a method of live-cell microfluidic microscopy, we determined that the minimum pheromone concentration required to establish polarity is 6 nM. When determining the minimum pheromone concentration required to maintain polarity, we observed that during a multi-step reduction of pheromone concentration most cells continued to hold polarity and cell cycle arrest at concentrations below 6 nM. In fact, a fraction of cells (~30%) held polarity and cell cycle arrest even after pheromone was completely removed. The difference between the minimum pheromone concentration required to establish polarity (~ 6 nM), and the minimum concentration required to maintain polarity (~ 0 nM), suggests that the polarity is bistable.

Surprisingly, cells will disassemble polarity rapidly after a one-step reduction in pheromone concentration to 5 nM or less. The finding that the number of steps taken to reduce

iii

the pheromone concentration determines whether cells maintain polarity is consistent with a model containing a slow-adjusting negative regulation and a fast-adjusting positive feedback. We confirmed this model by successfully testing two predictions – that whether cells lose polarity after a one-step pheromone reduction and the rate at which polarity disassembly occurs will depend on the initial pheromone concentration.

Our studies have shown that pheromone regulated polarity is bistable. We also confirmed a model of slow-adjusting negative regulation and fast-adjusting positive feedback that plays a role in this mechanism of memory. The presence of bistability in pheromone regulated polarity is informative to the study of polarity in other organisms and will inform future mathematical models.

To my grandparents, Avner, Dov, Ester and Yardena, whose dreams were fulfilled by their grandchildren.

ACKNOWLEDGEMENTS

TABLE OF CONTENTS

LIST OF TABLES

LIST OF FIGURES

LIST OF ABBREVIATIONS AND SYMBOLS

μm	Micro meter
BAR	Barrier
BEM	Bud Emergence
bp	Base pair
CDC	Cell Division Cycle
CDF	Cumulative Distribution Function
CLA	Cln Activity dependent
DIC	Differential Interference Contrast
DNA	Deoxyribonucleic acid
DSE	Daughter-Specific Expression
FAR	Factor Arrest
FUS	Cell Fusion
G protein	Guanine nucleotide-binding protein
GAP	GTPase Activating Protein
GDP	Guanosine diphosphate
GEF	Guanine nucleotide Exchange Factor
GFP	Green Fluorescent Protein
GIC	GTPase Interactive Components
GTP	Guanosine triphosphate
Gα	G protein alpha subunit
Gβ	G protein beta subunit
Gγ	G protein gamma subunit

Hrs	Hours
Kb	kilobase pair
Kd	Dissociation Constant
KSS	Kinase Suppressor of Sst2 mutations
LatA	Latrunculin A
MAP	Mitogen-Activated Protein
MAP2K	Mitogen-activated protein kinase kinase
MAP3K	Mitogen-activated protein kinase kinase kinase
MAPK	Mitogen-activated protein kinase
MATa	Mating type a
MATα	Mating type α
Myo	Myosin
nM	Nano mol/L
p	Promoter
PAK	p21-Activated Kinase
PBD	Protein Binding Domain
PCR	Polymerase Chain Reaction
RAC	Ras-related C3 botulinum toxin substrate
RAS	Rat Sarcoma
RFP	Red Fluorescence Protein
RGA	Rho GTPase Activating
Rho	Ras Homolog family member
SCD	Synthetic Complete medium containing Dextrose

Sec   Second

SEM   Standard Error of the Mean

SKM   STE20/PAK homologous Kinase related to Morphogenesis

STE   Sterile

td   Tandon Dimeric

yom   Yeast Optimized Monomeric

YPD   Yeast Extract Peptone Dextrose growth medium

Δ   Deletion

CHAPTER 1 – INTRODUCTION

Introduction to Polarity

In the context of cell biology, polarity establishment refers to the transition from a homogenous spatial distribution of a molecular component to an asymmetrical one. Most typically the term applies to the formation of a cell front and back or top and bottom. The molecular components that become polarized typically include cytoskeletal proteins such as actin cables, as well as signaling molecules associated with polarity, such as Rac, Rho and Ras proteins. Polarity establishment is required for many different physiological processes, such as cell migration, morphogenesis and differentiation. Dysregulation of polarity can often lead to diseases. For instance, polarity pathways are often perturbed by oncogenic signaling. Loss of polarity is one of the hallmarks of cancer, causing cancer cells to display alterations of cell shape, cell-cell adhesion, and cell motility. These qualities are likely important for numerous aspects of malignant transformation and play a key role in cancer metastasis (Bardwell, 2004; Iden & Collard, 2008; M. Lee & Vasioukhin, 2008)

Cell polarity often occurs in the context of gradient tracking, in which cells polarize in response to an external chemical gradient that may change in intensity, duration, or directionality over time. Polarity in response to an external cue is crucial for T-cell's response to pathogens, fibroblast migration toward wound sites, and neuron growth toward nerve growth factor during development (Skupsky, Losert, & Nossal, 2005). Since the external cellular environment is dynamic and constantly changing, cells require regulatory mechanisms that allow them to

1

maintain a stable polarity patch while still being able to reorient their direction of polarity in response to changing environmental conditions. The signaling motifs that allow cells to adapt to changes in the cue are unknown. Elucidating and characterizing these regulatory mechanisms will have important implications for understanding complex cellular processes, such as chemotaxis and nerve growth.

Computational Models of Polarity

Various mathematical models describing polarity establishment have been proposed. A broad class of models invoke purely biochemical mechanisms that only require interactions between signaling molecules to generate spatially asymmetric concentration profiles (Causin & Facchetti, 2009; Goryachev & Pokhilko, 2008; Howell et al., 2012; Skupsky et al., 2005; Wedlich-Soldner, Altschuler, Wu, & Li, 2003). These models rely on positive feedback to amplify localized noisy regions of pathway activity and polarize through "diffusion-driven instabilities" that do not require directed transport or force generation. These models do, however, require chemical species that diffuse at different rates to keep pathway activity localized and prevent activity from spreading throughout the cell. Different diffusion rates are achieved by pathway components transitioning from the cytosol, where diffusion is fast, to the membrane, where diffusion is slow.

Models for diffusion-driven symmetry breaking can be further subdivided into two categories, monostable and bistable. Monostable models have one stable steady state for each stimulus level (Fig. 1.1A). Their dosage-response curves typically have a sigmoidal shape created by the positive feedback. In these models the positive feedback is sufficient to amplify the model's response to small fluctuations in the stimulus and establish a polarize state. In contrast, in bistable models the strong positive feedback results in the existence of two stable

steady states, and cells can exist in either a polarized or unpolarized state for a range of stimulus strengths (Fig.1.1B). Bistability is a mechanism of memory, as which steady state is observed depends on past conditions. The differences between monostable and bistable models also have biological implications. Monostable models have high sensitivity, and small perturbations in stimulus can cause cells to establish or lose polarity. Therefore, monostable models can be much more reactive to changes in stimulus and allow cells to adapt to their environment quickly. Bistable models are much more robust and a larger, finite perturbation is required to initiate the polarization process. These models also feature a mechanism memory and maintain polarity against small fluctuations of stimulus once polarity is established (Ferrell, 2002; Ferrell & Xiong, 2001; Tyson, Chen, & Novak, 2003). Bistable regulation of polarity has also been suggested to improve sensitivity to shallow noisy gradients and to be the underlying mechanism behind spontaneous symmetry breaking, in which a cell polarizes in response to a spatially homogenous stimulus (Narang, 2006; Subramanian & Narang, 2004). Despite the distinct differences between models and the biological implications of favoring one model class over another, bistable or monostable regulation of polarity has not been determined experimentally.

Different models make different assumptions about the number of stable steady states the system has. Wave-Pinning models assume bistability. The solution to this model takes the form of a traveling wave, or a moving front, where the activity of the polarity protein of interest spreads like a traveling wave. The wave eventually stalls, or is pinned, due to substrate depletion of the inactive form of the molecular species. Since wave-pinning models rely on wave propagation, these models can establish polarity at a much faster rate compared to other model designs (Mori, Jilkine, & Edelstein-Keshet, 2008; Semplice, Veglio, Naldi, Serini, & Gamba, 2012).

While wave-pinning models rely on bistability to establish polarity, Turing models can either be monostable or bistable. These models were first developed by the famous mathematician Allen Turing (Turing, 1952). They rely on amplification of small local perturbations as their main polarity establishment mechanism. Turing models do not require bistability to be able to establish polarity, they can either be monostable or bistable, depending on the parameters used (Goryachev & Pokhilko, 2008; Howell et al., 2012; Onsum & Rao, 2007; Savage, Layton, & Lew, 2012). Experimentally determining whether polarity is regulated in a bistable or monostable manner will help guide future modeling efforts and give a preference to one class of models over another.
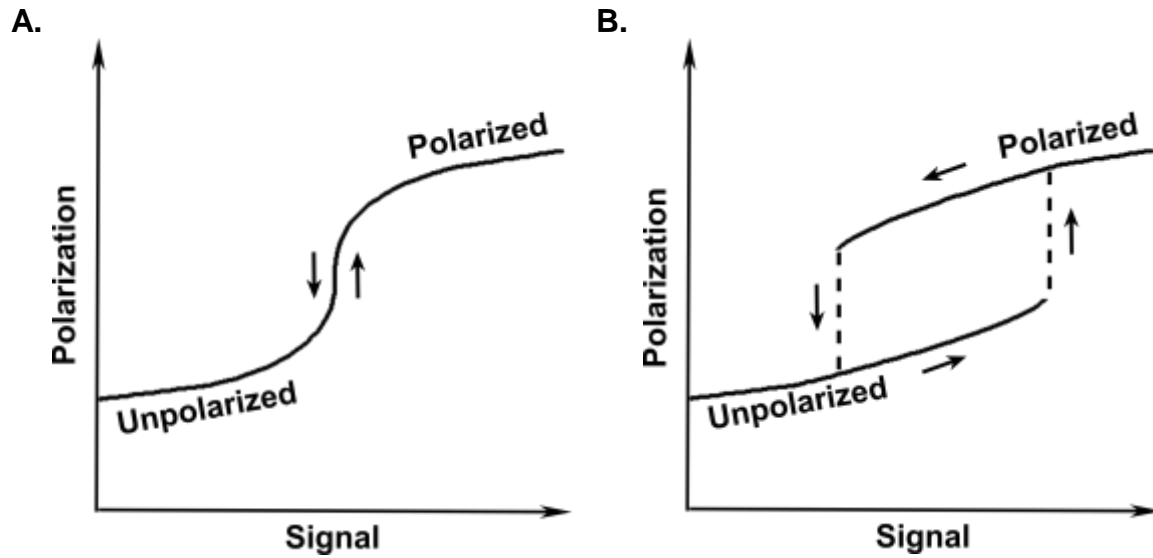
Fig. 1.1 Dosage-Response Curves for Monostable and Bistable Models. **(A)** Monostable positive-feedback models have sigmoidal-shaped curves created by the strong positive feedback. **(B)** Bistable models have curves with two branches due to the existence of two stable steady states for a range of signal strengths. The dominance of one steady state over another depends on the history of the system, as indicated by the arrows.

Budding Yeast as a Model Organism for the Study of Polarity

The small Rho GTPase Cdc42 plays a central role in polarity establishment in all eukaryotic cells. Many computational models for regulation of Cdc42 polarity establishment have been proposed (Howell et al., 2012; Layton et al., 2011; Slaughter, Das, Schwartz, Rubinstein, & Li, 2009; Wedlich-Soldner et al., 2003). However, to date a systematic study to determine if the polarity circuit of any cell type is bistable has not been carried out. Saccharomyces cerevisiae (budding yeast) is an ideal model organism for the study of polarity establishment. Budding yeast is a genetically tractable organism with relatively well-characterized signaling pathways. At the same time, budding yeast shares many of its signaling components with other eukaryotes. Specifically, human Cdc42 can functionally substitute for its yeast counterpart, indicating that key functions of Cdc42 have been highly conserved (Shinjo et al., 1990).

Budding yeast can exist either as a diploid or as a haploid with two mating types – a and α. Haploid cells secrete pheromone that attracts the opposite mating type and promotes cellular processes required for diploid formation. A yeast haploid cell at G1 can proceed through the cell cycle and polarize to establish a bud. Alternatively, in the presence of pheromone secreted from the opposite mating type, the cell will arrest in the G1 phase of the cell cycle and initiate the mating process. If the mating partner is nearby and high pheromone concentration is detected, the cell will form mating projections known as shmoos. If the mating partner is further away, the cell will undergo chemotropism and grow towards the potential mate, elongating into a worm-like shape (Fig. 1.2). Both budding and mating require polarity establishment to initiate the morphological changes associated with budding, shmoo-formation or chemotropism (Arkowitz, 2009; Bardwell, 2004).

Fig. 1.2 Budding Yeast in Different Mating States. *BAR1* yeast cells inside our microfluidic chamber with a 0-150 nM pheromone gradient. Cells on left continue to bud, cells in center show chemotropic growth, cells on the right form mating projections.

The mating pathway contains a Mitogen Activated Protein Kinase (MAPK) cascade, which is the first MAPK cascade discovered. MAPK cascades are an important, well studied signaling motif that is conserved across eukaryotes. It consists of a MAP3K (in budding yeast, Ste11) that phosphorylates a MAP2K (Ste7) which phosphorylates a MAPK (Fus3), which then regulates downstream targets (Arkowitz, 2009; Bardwell, 2004). MAP kinase cascades are integral to many different types of cellular responses, such as proliferation (Geest & Coffer, 2009; Raffetto, Vasquez, Goodwin, & Menzoian, 2006; Shapiro, 2002; Zhang & Liu, 2002), differentiation (Chen, Deng, & Li, 2012; Oeztuerk-Winder & Ventura, 2012), and development (Bradham & McClay, 2006; Krens, Spaink, & Snaar-Jagalska, 2006; Oeztuerk-Winder & Ventura, 2012). These cascades often regulate polarity and cytoskeletal organization. The presence of such a well-conserved signaling cascade makes the mating pathway a great model for the study of polarity, since the results are relevant to polarity-related MAP kinase pathways in other organisms.

Budding yeast has been extensively used to study and computationally model polarity establishment in response to an internal static cue during budding (Howell et al., 2012; Layton et al., 2011; Marco, Wedlich-Soldner, Li, Altschuler, & Wu, 2007; Okada et al., 2013; Slaughter et al., 2009). Additionally, the components contributing to the positive feedback loop regulating polarity in yeast have been identified and also modeled (Bose et al., 2001; Irazoqui, Gladfelter, & Lew, 2003; Kozubowski et al., 2008; S. E. Smith et al., 2013).

Polarity establishment in yeast during mating has also been modeled recently. Several papers modeled gradient tracking and polarity reorientation in this pathway (Chou, Nie, & Yi, 2008; Dyer, Savage, Jin, & Zyla, 2013; Lakhani & Elston, 2017; McClure et al., 2015; Yi, Chen, Chou, & Nie, 2007). Since pheromone-regulated polarity in yeast is controlled by an external

stimulus that can easily be manipulated under laboratory conditions, the mating pathway of budding yeast can offer unique opportunities to experimentally study Cdc42 polarization and its role in gradient tracking. The body of computational work already done on polarity establishment in this pathway and organism will ensure the results will be relevant for the polarity field as a whole.

Cdc42 is an Important Polarity Protein

Cdc42 is a small regulatory GTPase of the Rho family that regulates the reorganization of the actin cytoskeleton. Cdc42 also modulates other signaling pathways that induces transcription (Johnson, Jin, & Lew, 2011; Madden & Snyder, 1998). During budding, Cdc42 is initially localized to the bud site, then to the bud tip and eventually localizes to the bud neck during cytokinesis. During mating, Cdc42 is localized to the shmoo or worm tip (Richman et al., 2004). Cdc42 is essential for successful cell replication. At restrictive temperature, a temperature-sensitive mutant of Cdc42 fails to bud, and instead forms large, arrested cells (Adams, Johnson, Longnecker, Sloat, & Pringle, 1990).

Cdc42 is a GTPase, and thus acts as a molecular switch for its downstream effectors. When bound to a GTP molecule, the GTPase is in its active state and will transduce the signal to downstream effectors. However, after GTP hydrolysis, the GTPase is inactive and bound to a GDP, effectively switching the GTPase off. The GTP hydrolysis reaction is often initiated by GTPase activating proteins (GAPs) that serve as negative regulators of the pathway. GTPases are activated by Guanine nucleotide exchange factors (GEFs), which leads to the dissociation of GDP from the GTPase, allowing the GTPase to associate with a GTP molecule and become active (Rikitake & Liao, 2005). The Cdc42 GEF in budding yeast is Cdc24 (Hartwell, Mortimer, Culotti, & Culotti, 1973) and the GAPs are Bem3, Rga1 and Rga2 (Bender & Pringle, 1991;

Madden & Snyder, 1998; G. R. Smith, Givan, Cullen, & Sprague, 2002; Stevenson et al., 1995; Zheng et al., 1993).

The Pheromone Response Pathway and Polarity Regulation

The signaling pathway for polarity establishment during mating is well-characterized (Fig. 1.3). Upon pheromone binding, the $G_\beta G_\gamma$ subunits are released from the large G-protein coupled to the pheromone receptor. The G_β subunit triggers the MAP kinase cascade resulting in the phosphorylation and activation of the MAP kinase Fus3. Fus3 activates transcription of pheromone-dependent genes – among them the polarity scaffold Far1. Additionally, Fus3 phosphorylates the Far1 protein, causing export of Far1 from the nucleus and protection of Far1 from degradation. Far1 inhibits the cyclin dependent kinase Cdc28, thereby arresting the cell cycle. Most significantly for polarization, Far1 forms a complex with Cdc24, the guanine nucleotide exchange factor (GEF) for Cdc42. The Far1-GEF complex is then recruited by the free G_β subunit resulting in the activation of Cdc42 proximal to activated pheromone receptors. Cdc42 then organizes the actin cytoskeleton and establishes polarity (Arkowitz, 2009; Bardwell, 2004).
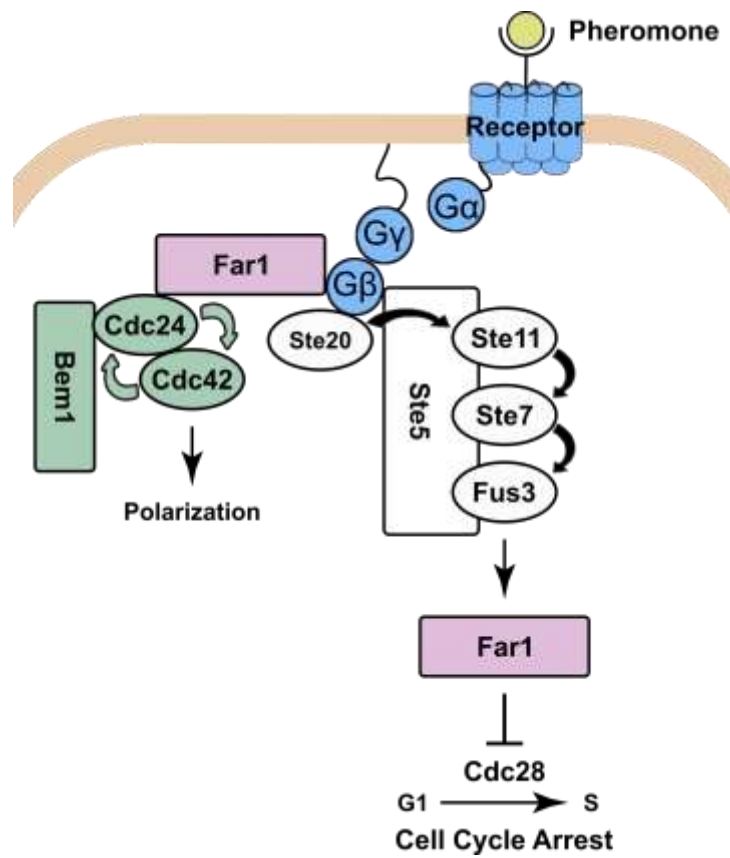
Fig. 1.3 Pathway Diagram for the Mating Pathway. Receptor and its coupled G protein are shown in blue. Components of the positive feedback regulating polarity shown in green.

The mating pathway has a well-characterized polarity positive feedback loop, mediated by a complex comprised of the Cdc42 GEF, Cdc24, and the scaffold, Bem1, which binds to active Cdc42. Activated Cdc42 recruits the Bem1-GEF complex, which in turn catalyzes the activation of more Cdc42. This results in robust positive feedback that can amplify a shallow, noisy stimulus gradient to maximal pathway activation (Bose et al., 2001; Irazoqui et al., 2003; Kozubowski et al., 2008; S. E. Smith et al., 2013).

Here we use the pheromone response pathway to show that Cdc42 polarity establishment is a bistable process that shows hysteresis. Unpolarized cells require 6 nM pheromone to establish polarity. In contrast, cells that established polarity in a high pheromone concentration will remain polarized through a multi-step reduction of pheromone concentration to 0 nM. Additionally, we demonstrate that polarized cells will lose their polarity if pheromone is sufficiently reduced in a one-step fashion. These results suggest a model of a positive feedback that adjusts to changes in pheromone concentration quickly, combined with a negative feedback that adjusts slowly. The model predicts that the pheromone concentration prior to a one-step decrease will determine whether cells will maintain or disassemble polarity, and at which rate. We show that these predictions hold experimentally, thus confirming the model.

CHAPTER 2 - MATERIALS AND METHODS

Experimental Design

To determine whether polarity establishment is a monostable or bistable process, we employed an approach integrating traditional yeast genetics and cutting-edge microfluidics-enabled microscopy with computational image analysis to resolve signaling mechanisms occurring at different time scales and provide a quantitative understanding of dynamic cell polarity. We first constructed a strain containing the polarity scaffold protein Bem1 tagged with yomNeonGreen fluorescent tag. The strain also contained a deletion of the *BAR1* gene coding for a protease that degrades pheromone (Barkai, Rose, & Wingreen, 1998; Ciejek & Thorner, 1979; Sprague & Herskowitz, 1981). Lastly, the strain also contained the myosin II light-chain Myo1 tagged with yomRuby red fluorescent protein. Since Myo1 localizes to the bud neck in all stages of the cell cycle with the exception of G1, the tag will allow us to exclude from our analysis cells that are going through the budding cycle (Fig. 2.4). We then employed a series of microfluidic microscopy experiments followed by rigorous image analysis to quantify the data and determine whether Cdc42 polarity is monostable or bistable. Following is a detailed description of the methods we employed.

Yeast Strains and Genetic Procedures

Table 2.1 lists yeast strains used in these studies. Table 2.2 lists the sequence of oligonucleotides used for PCR fragment amplification, mutagenesis, and DNA sequence confirmation involved in the construction of these strains. Media preparation and standard yeast

genetic methods for transformation, gene replacement, crosses, and tetrad dissection were as

described in Amberg *et al.*(2005).

Table 2.1 Budding Yeast Strains Constructed in this Study

Strain	Genotype	Source
BY4741	*MAT**a** his3Δ₁ leu2Δ₀ LYS2 met15Δ₀ ura3Δ₀*	Brachmann et al., 1998
BY4741-112	*MAT**a** his3Δ₁ leu2Δ₀ LYS2 met15Δ₀ ura3Δ₀ bar1Δ::hisG-URA3-hisG*	This study
BY4741-120	*MAT**a** his3Δ₁ leu2Δ₀ LYS2 met15Δ₀ ura3Δ₀ bar1Δ::hisG URA3*	Cloned by M Peña
BY4741-124	*MAT**a** his3Δ₁ leu2Δ₀ LYS2 met15Δ₀ ura3Δ₀ bar1Δ::hisG-URA3-hisG*	This study
BY4741-172	*MAT**a** his3Δ₁ leu2Δ₀ LYS2 met15Δ₀ ura3Δ₀ GIC2^{W23A}PBD-1.5tdTomato::His5 bar1Δ::hisG*	This study
BY4741-175	*MAT**a** his3Δ₁ leu2Δ₀ LYS2 met15Δ₀ ura3Δ₀ bar1Δ::hisG*	This study
BY4741-183	*MAT**a** his3Δ₁ leu2Δ₀ LYS2 met15Δ₀ ura3Δ₀ bar1Δ::hisG BEM1-yomNeonGreen::CgHIS3*	This study
BY4741-187	*MAT**a** his3Δ₁ leu2Δ₀ LYS2 met15Δ₀ ura3Δ₀ bar1Δ::hisG-URA3-hisG BEM1-yomNeonGreen::CgHIS3*	This study
BY4741-191	*MAT**a** his3Δ₁ leu2Δ₀ LYS2 met15Δ₀ ura3Δ₀ bar1Δ::hisG-URA3-hisG BEM1-yomNeonGreen::CgHIS3 MYO1-yomRuby2Kan^{r}*	This study
BY4741-198	*MAT**a** his3Δ₁ leu2Δ₀ LYS2 met15Δ₀ ura3Δ₀ bar1Δ::hisG Bem1-yomNeonGreen::CgHIS3 MYO1-yomRuby2Kan^{r}*	This study
BY4741-208	*MAT**a** his3Δ₁ leu2Δ₀ LYS2 met15Δ₀ ura3Δ₀ bar1Δ::hisG Bem1-yomNeonGreen::CgHIS3 MYO1-yomRuby2Kan^{r} Cdc24-35A*	This study
BY4741-230	*MAT**a** his3Δ₁ leu2Δ₀ LYS2 met15Δ₀ ura3Δ₀ bar1Δ::hisG Bem1-yomNeonGreen::CgHIS3 MYO1-yomRuby2Kan^{r} bem3Δ::hphNT1*	This study
BY4741-232	*MAT**a** his3Δ₁ leu2Δ₀ LYS2 met15Δ₀ ura3Δ₀ bar1Δ::hisG Bem1-yomNeonGreen::CgHIS3 MYO1-yomRuby2Kan^{r} rga2Δ::Nat6MX*	This study

BY4741-234	*MAT**a** his3Δ₁ leu2Δ₀ LYS2 met15Δ₀ ura3Δ₀* *bar1Δ::hisG* *Bem1-yomNeonGreen::CgHIS3* *MYO1-yomRuby2Kan^r* *rga1Δ::hphNT1*	This study
BY4742	*MATα his3Δ₁ leu2Δ₀ lys2Δ₀ MET15 ura3Δ₀*	Brachmann *et al.*, 1998
BY4742-32	*MATα his3Δ₁ leu2Δ₀ lys2Δ₀ MET15 ura3Δ₀* *bar1Δ::hisG-URA3-hisG*	This study
BY4742-51	*MATα his3Δ₁ leu2Δ₀ lys2Δ₀ MET15 ura3Δ₀* *bar1Δ::hisG* *BEM1-yomNeonGreen::CgHIS3*	This study
BY4742-56	*MATα his3Δ₁ leu2Δ₀ lys2Δ₀ MET15 ura3Δ₀* *bar1Δ::hisG* *BEM1-yomNeonGreen::CgHIS3* *MYO1-yomRuby2Kan^r*	This study

Table 2.2 Oligonucleotides Used in this Study

Oligo	Sequence	Application
562	GCAACCTGACCTACAGG	Used with 1258 to confirm tagging of *MYO1* with yomRuby2::Kan^r
704	GGA AGT TCT GAA GTC CCA AGC A	Used with 1000 to confirm integration of plasmid at *URA3* location
947	TGGCCGCATCTTCTCAAATA	Used with 1214 to confirm excision of *URA3*
966	CTGCCTCTCCAGTTGTCATG	Used with 967or 972 to confirm replacement of *BAR1* with *hisG-URA3-hisG*
967	CAGCAAAATAGCATTCCTTGG	Used with 966 or 968 to confirm replacement of *BAR1* with *hisG-URA3-hisG*
968	CAGCTCTTGCTTGCTCTGTG	used with 967 to confirm replacement of *BAR1* with *hisG-URA3-hisG*
972	GTGCGTGATGATGACATTCC	Used with 967 to confirm replacement of *BAR1* with *hisG-URA3-hisG*
1000	CCCAACTGCACAGAACAAAA	Used with 704 to confirm integration of plasmid at *URA3* location
1097	TCA GAA ACT TCT CGA CAG AC	Used with 1414 or 1442 to confirm deletion of *CDC24* or *BEM3*, respectively.
1148	AGGAGCCGTAATTTTTGCTT	Used with primers 1448 or 1468 to confirm *RGA1* or *RGA2* deletion, respectively. Anneals to t-TEF region.
1214	GATGTTAGCAGAATTGTCATGCAAGG	Used with 947 to confirm excision of *URA3*
1255	AAAGGATATAAAGTCTTCCAAATTTTTAAAAAAAAGTTCGATCGATGAATTCGAGCTCG	Used with 1316 for 1st round PCR to amplify *yomRuby2::Kan^r* and create homology to *MYO1*
1256	TCTGGAAAAGCCGTTATGAATCTACCATGATAGGCTCGAAAAATATTGATAGTAACAATG	Used with 1257 for 2nd round PCR to amplify *yomRuby2::Kan^r* and extend homology to *MYO1*
1257	TTCTGTATATACAAAACATCTCATCATTATTTTTTTAAATAAAGGATATAAAGTCTTCCA	Used with 1256 for 2nd round PCR to amplify *yomRuby2::Kan^r* and extend homology to *MYO1*
1258	GAA GCG AAT TTG AGG AAG CTA CTT TG	Used with 562 to confirm tagging of *MYO1* with *yomRuby2::Kan^r*
1294	CATCATAGATATTGCCACGGGG	Used with 1300 to amplify 1 kb upstream of the *BEM1* stop codon
1297	CCTATGTGCATCTGCCAAGTAAATCATCGATGAATTCGAGCTCG	Used with 1298 to amplify yo*mNeonGreen::CgHIS3* and create homology to *BEM1*

1298	CGAGCTCGAATTCATCGATGATTT ACTTGGCAGATGCACATAGG	Used with 1297 to amplify yo*mNeonGreen::CgHIS3* and create homology to *BEM1*
1299	AGGGACTCACATCTATCTTGGG	Used with 1301 to amplify 1 kb downstream of the *BEM1* stop codon
1300	GGCTTGGATTATGTTACTGACTTGT G	Used with 1294 to amplify 1 kb upstream of the *BEM1* stop codon
1301	TTACTTGGCAGATGCACATAGG	Used with 1299 to amplify 1 kb downstream of the *BEM1* stop codon
1316	AAATATTGATAGTAACAATGCACA GAGTAAAATTTTCAGTGGTGCTGG TTTAATTAAC	Used with 1255 for 1st round PCR to amplify yo*mRuby2::Kan^r* and create homology to *MYO1*
1354	AATTGGTCGACTTGGAGGGC	Used with 1360 to confirm tagging of *BEM1* with yo*mNeonGreen::CgHIS3*
1360	CCAGCACCAGCACCTGC	Used with 1354 to confirm tagging of *BEM1* with yo*mNeonGreen::CgHIS3*
1414	GCAGAAGAGTACCATTGCTGTTAT C	Used with 1097 to confirm replacement of *CDC24* with *pCORE-UK*
1426	TCCAACCCGAGAGATCATGGCGAT CCAAACCCGTTTTGCCCCGCGCGT TGGCCGATTCAT	Used with 1427 to amplify *pCORE-UK* and create homology to 2999 bp in *CDC24*
1427	AATCCCCATCTTCGTCCTGATATTT GATCTTGGTGATTGGTTCGTACGC TGCAGGTCGAC	Used with 1426 to amplify *pCORE-UK* and create homology to 2999 bp in *CDC24*
1430	CCCCTGTTGGTCAAAGAATTGC	Used with 1431 to amplify a 1kb fragment that could be cut with PstI to screen for *CDC24-35A* transformants
1431	GCGGCTGTTGTGATGATTCG	Used with 1430 to amplify a 1kb fragment that could be cut with PstI to screen for *CDC24-35A* transformants
1432	TGTTGCCTAGCCCTATCAAGACC	Used with 1433 to amplify cdc24-35A for TOPO cloning and sequencing
1433	CAAAATCCCCATCTTCGTCCTG	Used with 1432 to amplify cdc24-35A for TOPO cloning and sequencing
1434	CTAACCGGGACGCTGCTGAC	Second primer used to sequence Cdc24-35A (first primer is the TOPO m-13 reverse primer)
1435	GACGCGTGGTCAACTGGAAG	Third primer used to sequence Cdc24-35A
1436	CCGCAAAACAACCGGTCA	Forth primer used to sequence Cdc24-35A
1438	GCCTTTTGTTCGAGTTCGTGATTAC ATCAGGCATATACAAGGTCGACGG ATCCCCGGG	Used with 1439 for 1st round PCR to amplify a pFA6 plasmid and create homology to *BEM3*
1439	ATGGAGGTTTACTGGCAACGTTAT ATTTCTACAATTTTAGATCGATGA ATTCGAGCTCG	Used with 1438 for 1st round PCR to amplify a pFA6 plasmid and create homology to *BEM3*

1440	TTTTTCTCTTTTCTTCTTTGTCCTTG CCTTCTACCATTTTGCCTTTTGTTC GAGTTCGTG	Used with 1441 for 2nd round PCR to amplify a pFA6 plasmid and extend homology to *BEM3*
1441	AAGCCTCTATACATCTCGCCCTCTT TCTATCATTAAATCAATGGAGGTT TACTGGCAACG	Used with 1440 for 2nd round PCR to amplify a pFA6 plasmid and extend homology to *BEM3*
1442	CGGCGGTGATGTTGGAAAAA	Used with 1097 to confirm deletion of *BEM3*
1444	AGCTGATTCAGGTACTAGTGGTGG AGAGAGCGGCATATTAAAGGTCG ACGGATCCCCGGG	Used with 1445 for 1st round PCR to amplify pFA6 plasmid and create homology to *RGA1*
1445	CAGTTCATATAAGGCGGCTCAATG CAGAACCGAGGATAGCGATCGAT GAATTCGAGCTCG	Used with 1444 for 1st round PCR to amplify pFA6 plasmid and create homology to *RGA1*
1446	ACATTTATCTCTATTATAGCTTTTT GTACAAGACAAGGATAGCTGATTC AGGTACTAGTG	Used with 1447 for 2nd round PCR to amplify pFA6 plasmid and extend homology to *RGA1*
1447	CCTGCTTAAGTCTGCGATTAAAAA AATAACGTTTCGATACAGTTCATA TAAGGCGGCTCA	Used with 1446 for 2nd round PCR to amplify pFA6 plasmid and extend homology to *RGA1*
1448	CAAAATACCGAAACGCCAAA	Used with primer 1148 to confirm *RGA1* deletion
1467	ACTATTTTCTTACTTTATTCTTTTTT CATATGATTTCTTATTTAATCTATC CTATGTTTA	Used with 1477 for 2nd round PCR to amplify pFA6 plasmid and extend homology to *RGA2*
1468	GGCAAGTTTGACGTTCACTG	Used with primer 1148 to confirm *RGA2* replacement with a pFA6 plasmid
1475	AACGTAGCATCTCAAGAGCAAGG AGATTTTGATGAAAAAAATGGTCG ACGGATCCCCGGG	Used with 1476 for 1st round PCR to amplify pFA6 plasmid and create homology to *RGA2*
1476	TTTAATCTATCCTATGTTTATTTAA CTTTTGCAAATCTGTAATCGATGA ATTCGAGCTCG	Used with 1475 for 1st round PCR to amplify pFA6 plasmid and create homology to *RGA2*
1477	ATTACCAAGAGTTCATTGTACTTTT AATAAAGTGAAATATAACGTAGCA TCTCAAGAGCA	Used with 1467 for 2nd round PCR to amplify pFA6 plasmid and extend homology to *RGA2*

The *bar1Δ* strain BY4741-112 was constructed from BY4741 using the one-step gene replacement method (Rothstein, 1983) to replace the *BAR1* locus. The replacement used the *Eco*RI–*Sal*I fragment from pJGsst1 (Reneke, Blumer, Courchesne, & Thorner, 1988) that carries the *bar1Δ::hisG-URA3-hisG* allele. Transformants were isolated using –Ura synthetic media plates. Replacement of the *BAR1* locus was confirmed with colony PCR analysis using yeast genomic DNA as template with primer pairs 967/968, 972/966 and 967/966. Strains BY4741-124 and BY4742-32 are segregants resulting from the cross of BY4741-112 and BY4742. Strain BY4741-175 was generated from the BY4741-124 strain by selection on 5-fluoroorotic acid (Life Technologies, Grand Island, NY) medium (Boeke, LaCroute, & Fink, 1984). This medium provides a positive selection for isolates in which the *URA3* marker is excised by recombination within the direct *hisG* repeats (Alani, Cao, & Kleckner, 1987). Successful excision was confirmed with colony PCR analysis using yeast genomic DNA as template with primers pairs 972/968 and 1214/947.

The *GIC2^{W23A}PBD-1.5tdTomato::His5* strain BY4741-172 was constructed from BY4741-120 also using the integrative plasmid YIp211-GIC2PBD-RFP (Tong et al., 2007) that was cut with the ApaI restriction enzyme (New England Biolabs, Ipswich, MA). Successful integration was confirmed with colony PCR analysis using yeast genomic DNA as a template with primers 1000/704.

The *BEM1-yomNeonGreen* strain BY4741-183 was constructed as follows. Plasmid pDML99 (Landgraf, Huh, Hallacli, & Lindquist, 2016) was used as a template for a PCR reaction with primer pair 1297/1298. Genomic DNA from strain BY4741-175 was used as a template for two PCR reactions to generate homology to 1kb downstream and 1kb upstream of the *BEM1* stop codon using primer pairs 1299/1301, and 1300/1294, respectively. The three PCR

products were assembled using Gibson Assembly (New England Biolabs, Ipswich, MA), and the resulting product was used for transformation of BY4741-175. Transformants were selected on – His synthetic media plates. The integration of *yomNeonGreen* at *BEM1* was confirmed with colony PCR analysis using yeast genomic DNA as template with primer pair 1354/ 1360. Strains BY4741-187 and BY4742-51 are segregants of a cross between BY4141-183 and BY4742-32. To confirm that the *BEM1-yomNeonGreen* fusion strain responded normally to pheromone, the morphology of BY4741-187 and BY4741-175 cells responding to 0 nM, 10 nM and 50 nM pheromone was compared. For this comparison, cells from the parallel cultures were fixed with 2% formaldehyde at 0, 2 and 5.5 hrs. The vegetative, chemotropic or mating competent morphology of the fixed cells was scored and quantified using a hemocytometer.

The *BEM1-yomNeonGreen MYO1-yomRuby2* strain BY4141-191 was created by transforming strain BY4741-187 with the *MYO1-yomRuby2-Kan^r* allele. Plasmid pFA6a-link-yomRuby2-Kan^r (S. Lee, Lim, & Thorn, 2013) was used a template for a first round PCR reaction with primer pair 1316/1255. The product of this reaction was used as a template for a second PCR reaction with primer pair 1256/1257. The resulting product was used for transformation of BY4741-187. Transformants were selected on complete media plates containing G418 (Sigma-Aldrich, St. Louis MO). Integration of *yomRuby2* at the *MYO1* locus was confirmed by colony PCR analysis using yeast genomic DNA as template with primer pair 1258/562. Strains BY4741-198 and BY4742-56 are segregants of a cross between BY4741-191 and BY4742-51. To confirm that BY4741-198 responded normally to pheromone, the morphology of cells exposed to pheromone was compared to that of BY4741-175 in the procedure described above except that cells were fixed at 0, 2 and 4 hrs.

The unphosphorylatable *CDC24-35A* mutant strain BY4741-208 was created by a serial transformation of a diploid resulting from a cross of strains BY4741-198 and BY4742-56. Because *CDC24* is an essential gene the transformation could only be done in a diploid containing two copies of *CDC24*. The first step was a transformation of the diploid with a *cdc24Δ::CORE-UH* allele that was generated in a PCR reaction using the pCORE-UH plasmid (Storici & Resnick, 2006) as a template with primers 1426/1427. Deletion of one of the copies of *CDC24* was confirmed by colony PCR analysis using yeast genomic DNA as template with primer pair 1414 and 1097. Plasmid pSW86 (Wai, Gerber, & Li, 2009) was digested with the restriction enzymes HindIII and HpaI (New England Biolabs, Ipswich, MA), and the resulting 2999 bp fragment was used to replace the *cdc24Δ::CORE-UH* allele. The transformation was confirmed with colony PCR analysis using yeast genomic DNA as template with primer pair 1430/1431 and a subsequent digestion of the product using the PstI restriction enzyme (New England Biolabs, Ipswich, MA). The diploid was then sporulated and subjected to tetrad analysis for the recovery of haploid segregants. Haploids containing the *CDC24-35A* allele were identified using the PstI restriction strategy described above. A DNA fragment from all segregants of interest was amplified with colony PCR using yeast genomic DNA as template with primer pair 1432/1433. The amplified fragment from each segregant was cloned into the pCR Blunt II Topo vector (Invitrogen Life Technologies, Grand Island, NY) and sequenced using M13R, 1434, 1435 and 1436 primers to ensure the presence of all mutation sites using the University of North Carolina – Chapel Hill Core Facilities.

The *bem3Δ::hphNT1* strain BY4741-230 was created by transforming strain BY4741-198. Plasmid pFA6a-hphNT1 (Hentges, Van Driessche, Tafforeau, Vandenhaute, & Carr, 2005) was used a template for a first round PCR reaction with primer pair 1438/1439. The product of

this reaction was used as a template for a second PCR reaction with primer pair 1440/1441. The resulting product was used for transformation of BY4741-198. Transformants were selected on complete media plates containing Hygromycin B (Sigma-Aldrich, St. Louis MO). Deletion of *BEM3* was confirmed by colony PCR analysis using yeast genomic DNA as template with primer pair 1441/1097.

The *rga2Δ::Nat6MX* strain BY4741-232 was also created by transforming strain BY4741-198. Plasmid pFA6a-Nat6MX (Hentges et al., 2005) was used a template for a first round PCR reaction with primer pair 1475/1476. The product of this reaction was used as a template for a second PCR reaction with primer pair 1477/1467. The resulting product was used for transformation of BY4741-198. Transformants were selected on complete media plates containing Nourseothricin (Sigma-Aldrich, St. Louis MO). Deletion of *RGA2* was confirmed by colony PCR analysis using yeast genomic DNA as template with primer pair 1468/1148.

The *rga1Δ::HphNT1* strain BY4741-234 was created by transforming strain BY4741-198. Plasmid pFA6a-hphNT1 (Hentges et al., 2005) was used a template for a first round PCR reaction with primer pair 1444/1445. The product of this reaction was used as a template for a second PCR reaction with primer pair 1446/1447. The resulting product was used for transformation of BY4741-198. Transformants were selected on complete media plates containing Hygromycin B (Sigma-Aldrich, St. Louis MO). Deletion of *RGA1* was confirmed by colony PCR analysis using yeast genomic DNA as template with primer pair 1448/1097.

Microfluidic Technology to Image Cell Response with a Fast Time-Resolution

The microfluidic device used has a simple design featuring four inputs, two at each side of the chamber, and four outputs located along the center of the device (Fig. 2.1). In the center of the device is a main chamber with a ceiling height of 3.6 µm, which is the area of the device

containing cells to be imaged. Two feeding channels flow on both sides and connect to the main chamber with microchannels that are 1.2 µm tall. The rest of the channels in the device are 10 µm tall. Cells are loaded into the device through the two middle output channels. The shorter ceiling in the main chamber causes the cells to stop their flow and remain stationary, while the microchannels feed media into the main chamber and replenish nutrients and pheromone. Once cell loading is complete, all output channels are used to collect excess media coming in from the input syringes, the feeding channels and the main chamber. A new chamber was used for every experiment. All chambers for this project were poured off of the same mold to ensure consistency among experiments and reduce error.

The two input ports on each side of the chamber are connected to syringes containing different concentrations of pheromone (or no pheromone at all). Changing the relative heights of the input syringes can change the concentration of pheromone flowing into the main chamber where the cells reside. The syringe heights can be manipulated so the cells see the pheromone concentration contained by either one of the syringes, or an intermediate pheromone concentration. The long and curvy features of the feeding channels ensure an intermediate pheromone concentration will be well-mixed before flowing into the main chamber. The height of the syringes was changed by an automatic robot built according to instructions from the Hasty lab Dial-A-Wave motor with hardware version 2 configuration (Ferry, Razinkov, & Hasty, 2011).
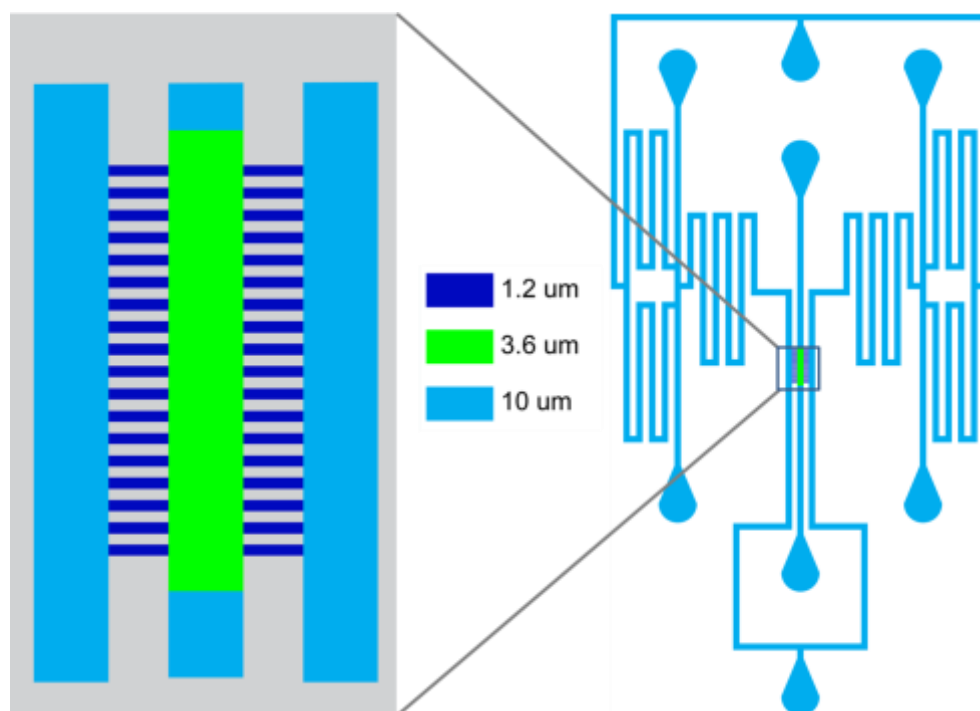
Fig. 2.1 Schematic of the custom microfluidic chamber. On left, enlargement of main chamber. Cell loading zone is in green and microchannels are in royal blue.

Using the microfluidic device allows quick pheromone concentration changes. The pheromone concentration within the main chamber changes within ̃10 sec of syringe height adjustment. The innovative experimental design results in single-cell quantitative data with the short time resolution needed to characterize cell response in real time.

Time-lapse imaging to follow pheromone-regulated polarity, morphology and cell cycle arrest

The experiments were done in microfluidic device and cell culturing methods as described in the supplement to Hao et al., 2008. An overnight cell culture was grown in synthetic complete medium. In the morning of the experiments, the culture was diluted and incubated for two doubling times. Prior to loading cells into the chamber, cells were counted and budding index was calculated to ensure the culture was in early log phase ($0.5-1\text{x}10^7$ cells/mL). The culture was then diluted to a cell density of $1-2\text{x}10^6$ cells/mL to optimize loading into the chamber and ensure consistent experimental conditions.

Alexa 647 (Thermo Fisher Scientific, Waltham, Massachusetts, USA) dye was added to pheromone containing media to track changes in pheromone concentrations throughout the experiment. Images of the dye at both junctions leading to the chamber were acquired and syringe positions were adjusted to ensure that pheromone flow would match from both sides of the chamber. Images of the dye in the main chamber were acquired during experimental set up to construct a calibration curve for the motor controlling the syringes. The chamber was imaged to ensure dye turned on and off within less than 20 seconds.

Microscopy was performed with an Olympus IX81 motorized inverted confocal spinning disk microscope using a Plan Apo N 60×/1.42 oil objective and a iXon ultra EMCCD camera. Acquisition was performed with MetaMorph software (Molecular Devices, Sunnyvale, CA). The 488 nm laser was set to 2% intensity, the 561 nm laser to 6% intensity, the 640 nm laser to 5%

intensity and the 450 nm laser to 0% intensity. GFP (488 nM) and differential interference contrast images of cells from seven different stage positions were taken every 5-minutes. RFP (651 nM) images were taken every 10 minutes and the dye (640 nM) was imaged every 25 minutes. In experiments where pheromone concentration was switched from a higher concentration (50 nM or 10 nM) to a lower concentration (0-6 nM) in one step, higher acquisition rates were used around the transition point. DIC and GFP images were acquired every 2.5 minutes starting 10 minutes prior to the concentration change and ending 30 minutes after the change. The acquisition interval for all other wavelengths was unchanged.

Cell segmentation and quantification of cell polarity

Image processing and cell scoring were aided by use of ImageJ software (Schneider, Rasband, & Eliceiri, 2012). A Gaussian filter with sigma of 1 was applied to the Images for all fluorescence channels to get rid of camera-related noise. A z projection of max intensity was used for all z stacks and a background subtraction with a radius of 50 was applied. Images were registered using the Descriptor Based Series Registration plugin. Registration for all channels was done based on the model found for the DIC series.

Inner boundaries between cells close to one another were extracted from the DIC series using the edge-detection function in MatLab (The MathWorks, 2015). Edges were detected using two different thresholds with the Sobel method. The less refined edges were then filled and eroded to create a mask that was smaller than the surface of the cells themselves. The eroded mask was used to multiply the refined edges detected using the algorithm, creating a mask that retained only the inner boundaries between cells and omitting the boundaries between cells and their environment.

The edge detection function was applied to the original DIC series again using the Sobel edge detection method with a coarse threshold. The edges were dilated, closed and filled in order to create a mask that was much larger than the cells themselves, minimize the areas of the images treated by the cell segmentation algorithm and speed up the data analysis process. Both masks (the inner boundary mask and the larger mask) were manually checked to ensure they correctly represented boundaries between cells and corrected when necessary. The two masks were then applied to the GFP images using a simple image multiplication in ImageJ.

Cells were then segmented using SegmentMe_2D (Fig. 2.2) (Tsygankov, Chu, Chen, Elston, & Hahn, 2014). The masked GFP movies were loaded to Segment Me. A dynamic filter was applied by averaging every image with the time points that preceded and followed it. An additional Gaussian filter of a size 15 and a σ=1 was applied to the images. Water shedding was then applied to the images using 45 different thresholds. After examination of the segmentation results, the single, most successful, threshold was chosen and used to segment the cells. The cells were then tracked through time in order to generate a single time series for every cell.
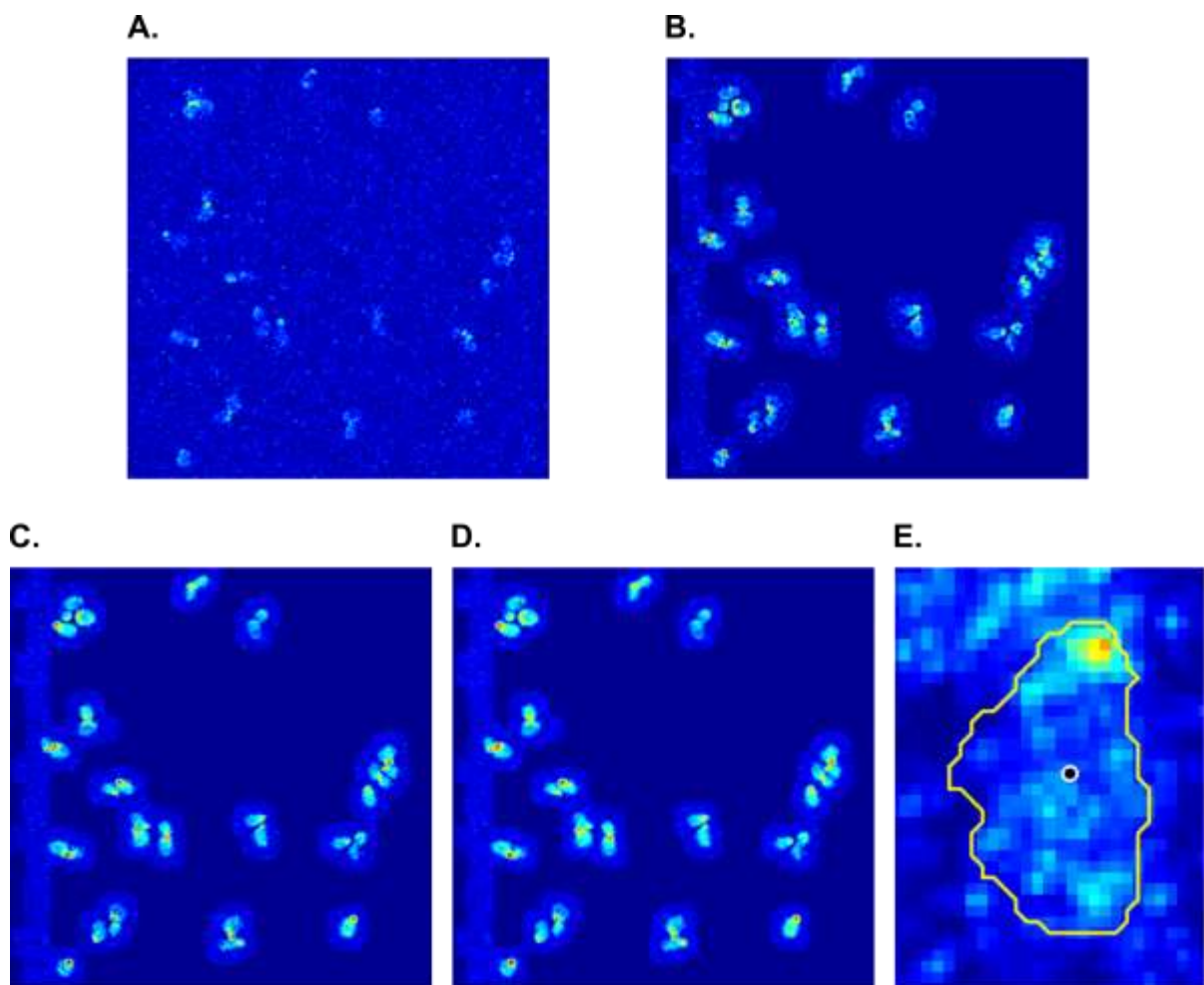
Fig. 2.2 Segmentation process for cells. (**A**) Raw GFP images (**B**) Image with DIC mask applied. (**C**) Image with dynamic filter applied (**D**) Image with Gaussian filter applied. (**E**) Single-cell raw data with the final segmentation mask applied in yellow.

Once the cells were segmented and tracked, the final masks were applied to the original registered background-subtracted GFP z-projection. The original data was quantified for each cell using SegmentMe_2D. Only cells that were determined to be in G1 by the absence of a visible Myo1-yomRuby spot at the beginning of the relevant time span were analyzed (Fig. 2.4). Single cell data was truncated when cells entered S phase of the cell cycle, as determined by the appearance of a visible Myo1 spot, and these cells were dropped from the mean for the following time points.

Different data quantification methods were compared to identify the most appropriate one. Methods that were examined included area of the polarity patch, mean intensity per pixel, total intensity of the cell, coefficient of variation of pixel intensity and deviation from uniformity. The method of deviation from uniformity was chosen, since it was the least sensitive to changes in total polarity protein expression, changes in cell size and changes in illumination conditions from one experiment to another. The method was also the most sensitive to changes in polarity protein distribution and captured small noisy fluctuations in polarity patch stability. Therefore, this method was the most sensitive to distribution changes while being the least sensitive to other variations between cells and experiments.
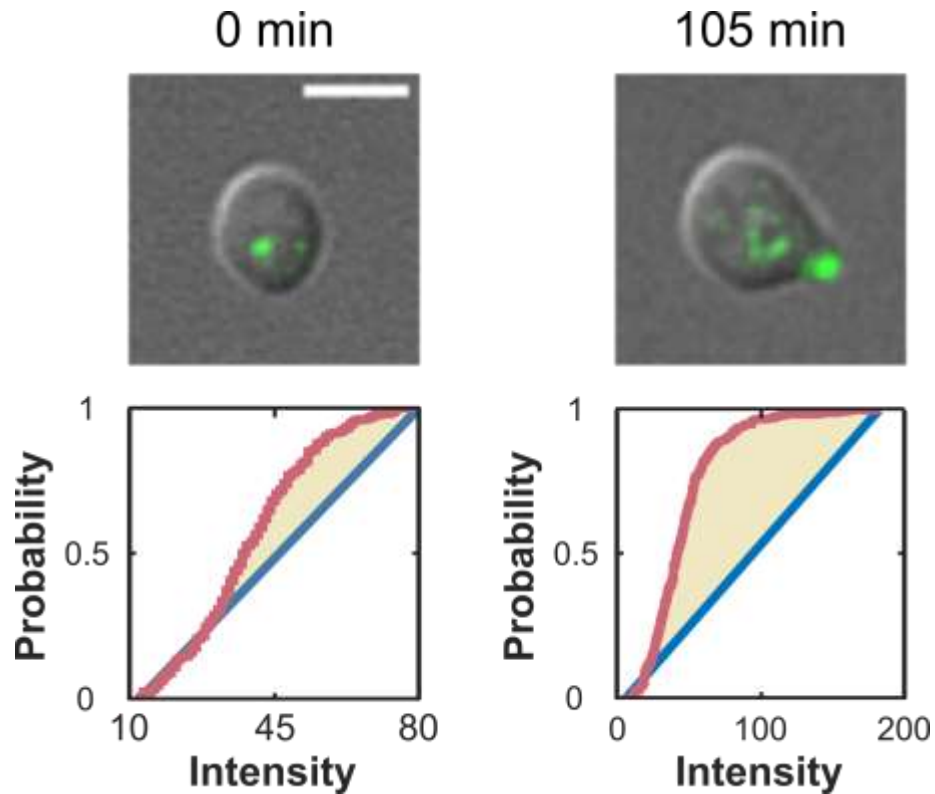
Fig. 2.3 Representative Cell Before and After Polarity Establishment and its Deviation from Uniformity. The upper panel shows a representative cell that was exposed to 50 nM pheromone and is shown at 0 min and at 105 min, after a tight polarity patch has been established. Bottom panels show the calculation of deviation from uniformity for both time points. Pink curves are the experimental CDF for pixel intensity. Blue curves are the CDF of an equivalent homogeneous distribution. The tan area between the curve is the integral on which the deviation from uniformity is based. At 0 min the cell has a deviation from uniformity of 0.209, and at 105 min one of 0.546.

Deviation from uniformity for fluorescence of the polarity marker (Bem1-yomNeonGreen) was calculated for each cell at each time point (Fig. 2.3) in SegmentMe_2D based on the Kolmogorov-Smirnov test to compare the experimental pixel distribution to an equivalent uniform homogenous distribution (Justel, Pefia, & Zamar, 1997; Tsygankov et al., 2014). For each segmented cell, at each time point, the highest (I_{max}) and lowest intensity (I_{min}) values were determined. A homogeneous uniform distribution was generated between these two values. The cumulative distribution function was calculated for the homogenous uniform distribution as well as the experimental pixel intensity distribution. The integral between the two cumulative distribution functions was taken and normalized to be a value between 0 and 1.

The procedure is captured in the following equations:

For a single segmented cell in a single time point, $I_{i,j}$

$$I_{min} = \min_{i,j} I_{i,j}$$

$$I_{max} = \max_{i,j} I_{i,j}$$

$$x_n = I_{min} + \frac{n-1}{N-1}(I_{max} - I_{min})$$

where $n = 1,2,\dots,N$ $i = 1,2,\dots,I$ and $j = 1,2,\dots,J$.

The cumulative intensity distribution is

$$y_n = \frac{1}{IJ}\sum_{i,j} H(I_{i,j}, x_n) \text{ where}$$

$$H(I_{i,j}, x_n) = \begin{cases} 1 \ if \ I_{i,j} < x_n \\ 0 \ if \ I_{i,j} \geq x_n \end{cases}$$

For a uniform homogenous distribution, the cumulative distribution is:

$$U_n \approx \frac{x_n - I_{min}}{I_{max} - I_{min}} = \frac{n-1}{N-1}$$

The deviation from uniformity is:

$$P = \frac{2}{N} \sum_{n=1}^{N} (y_n - U_n)$$

$$y_n \in [0,1], P \in [0,1]$$

The mean of the deviation from uniformity for all cells was taken and the standard error calculated for each time point. The mean +/- standard error were plotted in Matlab (The MathWorks, 2015).

To determine the maximum deviation from uniformity cells achieved while in the G1 stage of the cell cycle, each single cell time trace was smoothed in Matlab (The MathWorks, 2015) using a 3 time point averaging window, and the trace was truncated either when the cell entered S-phase or after 2 hrs., whichever came first. The maximum value for each smoothed single cell trace was determined in Matlab and the results were plotted as a box and whiskers plot.

Identification and quantification of G1 cells

Myo1 is a myosin II subunit that is required for actomyosin contractile ring contraction and cell separation after cytokinesis. Myo1 localizes to the bud neck between the S-phase of the cell cycle and the completion of cytokinesis and is visible by microscopy in all stages of the cell cycle but G1. The length of time each cell remained in the G1 phase of the cell cycle was determined by eye based on the appearance of a Myo1-yomRuby spot when a cell entered the S-phase of the cell cycle. The results were plotted as a box and whiskers plot in Matlab (The MathWorks, 2015). The percent of cells in the G1 phase of the cell cycle was determined for each replica of the experiment. The results for the three replicas were averaged for each time point and the standard error was calculated. The mean +/- standard error were plotted in Matlab.
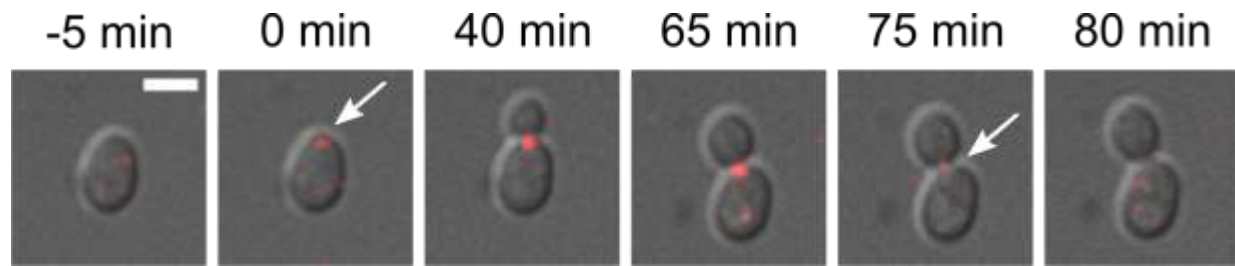
Fig. 2.4 Myo1-Ruby is an indicator of cell-cycle progression. Panel shows a representative cell that was imaged in the absence of pheromone in a microfluidic chamber. Myo1 clearly localizes to the bud neck in all stages of the cell cycle with the exception of G1. The points of cell cycle entry and exit are indicated by a white arrow pointing to Myo1 localization.

Statistical analysis was used to determine statistically significant differences between different dosages' maximum deviation from uniformity and length of time cells spent in G1. First, a Levene Absolute multiple-sample test for equal variance was used in Matlab to determine if the homogeneity of variance assumption was violated. Since all data sets violated the assumption, a Welch F test was run using IBM SPSS. Since the test showed significant differences for all data, a Games-Howell post hoc test in IBM SPSS was used to determine which data sets are significantly different from each other (IBM Corp., 2011).

CHAPTER 3 – RESULTS

Polarity Establishment Requires 6 nM Pheromone

One of the hallmark features of a bistable system is hysteresis. Hysteresis refers to a mechanism of memory in which the observed response of a system depends on its history (Fig. 1.1). Therefore, we designed experiments to look for hysteretic behavior in pheromone-regulated polarity. In particular, we asked if the minimum pheromone concentration required to establish polarity is greater than the minimum pheromone concentration required to maintain an existing polarity patch. To answer this question, we used live-cell imaging performed in microfluidic chambers designed to allow precise temporal control of pheromone concentration. To visualize polarity assembly and disassembly, we tagged the scaffold protein Bem1 with a yomNeonGreen fluorescent tag. To quantify the degree to which individual cells polarize, we calculated the deviation from uniformity for fluorescently tagged Bem1. The deviation from uniformity measures the amount that the experimentally determined fluorescence distribution within a single cell deviates from a uniform distribution at a given time point (Fig. 2.3).

Cells can establish polarity through either the pheromone pathway during the G1 phase of the cell cycle, or as part of the cell cycle during the G1 to S phase transition. To ensure that only cells that polarized in response to pheromone were included in our analysis, we tagged the Myo1 subunit of Myosin II with a yomRuby2 fluorescent tag. Myo1 localizes to the bud neck during all stages of the cell cycle except G1 (Fig. 2.4). Therefore, our analysis only included unbudded cells lacking localized Myo1.

We first determined the minimum pheromone concentration required for naïve cells to polarize. To make this determination, we monitored polarity establishment for cells exposed to six pheromone concentrations (Fig. 3.1A-C). Cells in the G1 stage of the cell cycle exposed to 0 nM and 4 nM responded similarly and failed to polarize before progressing through the cell cycle. At 5 nM, cells showed a heterogeneous response, with some cells establishing a weak polarity patch, while others remained unpolarized. The cells that established polarity showed a very unstable polarity patch that appeared and disappeared throughout the experiment. At 6 nM the majority of cells established a weak yet stable polarity patch, but the polarization process was slow (~80 mins). Polarity establishment proceeded in a similar fashion at 10 and 50 nM. However, at these high concentrations of pheromone cells established polarity more quickly (~40 min) and in a switch-like manner. One possible explanation for the difference in the polarization rate between 6 nM and the higher doses, is that 6 nM is near the transition point, close to the sigmoidal slope or close to where the polarity circuit switches from a bistable to a monostable system (Fig. 3.1A and B, respectively), and molecular-level fluctuations are required to activate the positive feedback and establish polarity. At higher doses that are further from the transition point, the positive feedback is activated much faster without relying on fluctuations. At all doses, there was a ~20 min delay before cells began to establish polarity, suggesting that polarity requires the accumulation of one or more pathway components.
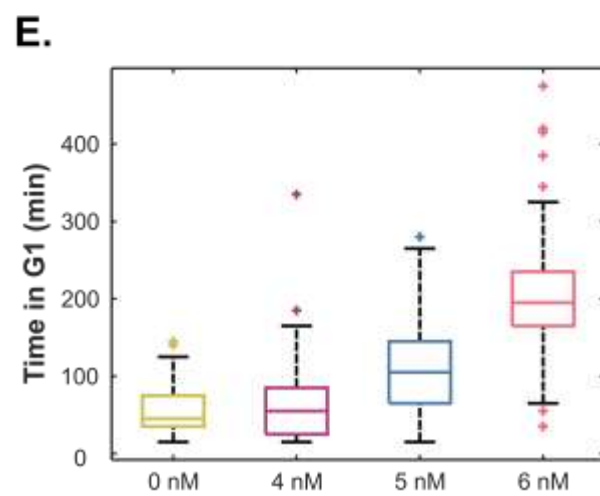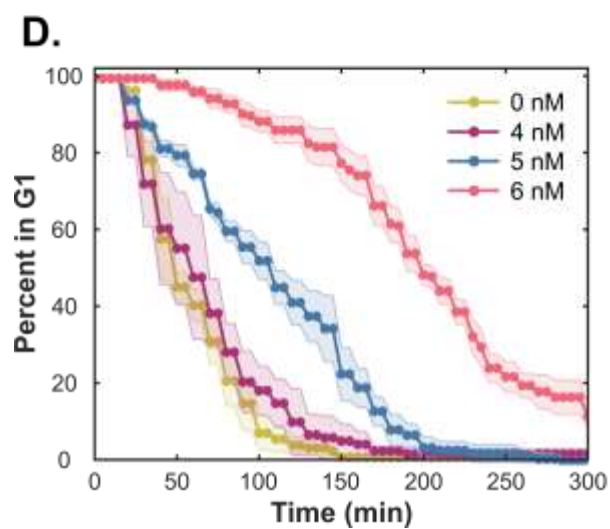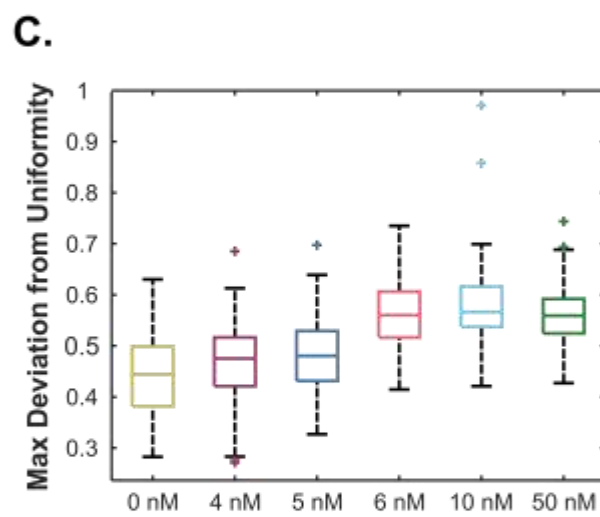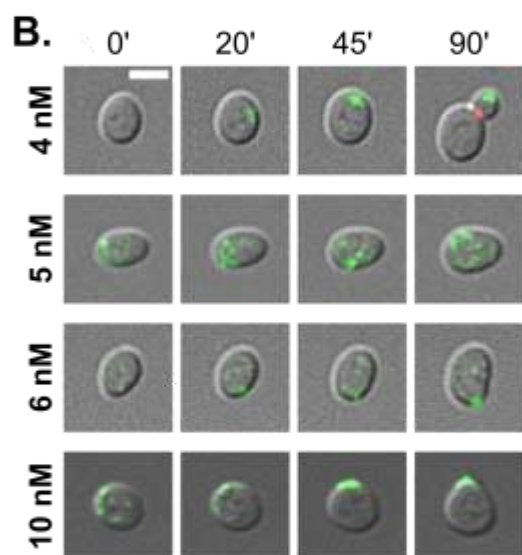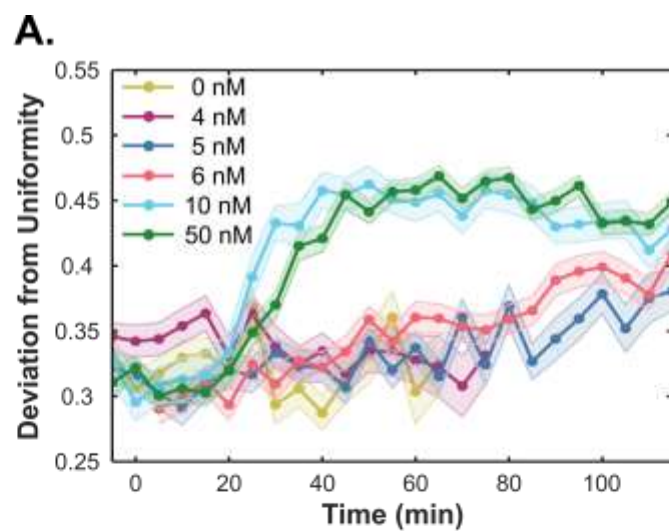
Fig. 3.1 Cells Establish Polarity at 6 nM and Arrest Cell Cycle at 5 nM. Cells at the G1 stage of the cell cycle were exposed to six pheromone concentrations, and both polarity establishment and cell cycle arrest were monitored. (**A**) Time traces for mean +/-standard deviation Bem1-yomNeonGreen deviation from uniformity after pheromone exposure. Curves show fast and switch like polarity establishment for 10 nM and 50 nM, and a slow, noisy one for 6 nM. (**B**) Representative cells for the 4 nM, 5 nM, 6 nM and 10 nM experiments. (**C**) The distribution of the highest level of deviation from uniformity cells achieved while being in G1 for each pheromone concentration. Box shows the upper and lower quartile, middle line is the median, whiskers extend to the most extreme data points not considered outliers and plus signs represent outliers. Results indicate that 6 nM is the lowest pheromone concentration at which significant polarization is achieved. (**D**) The mean percentage +/- standard error of cells remaining in G1 stage of the cell cycle over time. 5 nM is the lowest pheromone concentration at which cell cycle arrest occurs. At 10 nM and higher cells remain arrested for the duration of the experiment. (**E**) The distribution of lengths of time cells stay in the G1 stage of the cell cycle after pheromone treatment. Results indicate that 5 nM is the lost pheromone concentration at which significant cell cycle arrest is achieved. Conventions in E are the same as specified in panel (**C**).

To further characterize differences in polarity at different pheromone concentrations, we plotted the distribution of maximum values of the deviation from uniformity each cell achieved while in G1 (Fig. 3.1C, Table 3.1, 3.2 and 3.3). A Welch's ANOVA test and a Games-Howell post hoc test run on these distributions showed which concentrations have a statistically significant difference in their mean deviation from uniformity. The distributions for 0 nM and 4 nM are similar and do not show a statistical difference, suggesting there is no pheromone-induced polarity at 4 nM. While the median remained similar for 5 nM, the range of response narrowed and shifted upward, as there are fewer cells that fail to establish polarity. There was a statistical difference between 5 nM and all other doses except 4 nM, suggesting 5 nM shows an intermediate level of pheromone-induced polarity. At 6 nM, 10 nM and 50 nM, the whole distribution shifts upward, indicating that the majority of cells polarized at these concentrations. There is no statistical difference between these three doses, suggesting 6 nM is close to the minimum concentration required for pheromone-induced polarization, although polarization occurs slowly at this concentration.

Table 3.1 Lavene's Test of Homogeneity of Variance for Maximum Deviation of Uniformity During Polarity Establishment

Levene Statistic	df1	df2	Sig.
3.953	5	709	.002

Table 3.2 Welch's Analysis of Variance (ANOVA) for Maximum Deviation of Uniformity During Polarity Establishment

	Sum of Squares	df	Mean Square	F	Sig.
Between Groups	1.817	5	.363	73.825	.000
Within Groups	3.491	709	.005		
Total	5.308	714			

Table 3.3 Games-Howell Test of Multiple Comparisons for Maximum Deviation of Uniformity During Polarity Establishment

Pheromone Concentration (nM)		Mean Difference (I-J)		Std. Error	Sig.	95% Confidence Interval	
I	J					Lower Bound	Upper Bound
0	4	-0.023		0.010	0.201	-0.051	0.006
	5	-.038*		0.010	0.002	-0.066	-0.010
	6	-.117*		0.010	0.000	-0.144	-0.089
	10	-.134*		0.012	0.000	-0.169	-0.099
	50	-.112*		0.008	0.000	-0.136	-0.088
4	0	0.023		0.010	0.201	-0.006	0.051
	5	-0.015		0.009	0.592	-0.042	0.012
	6	-.094*		0.009	0.000	-0.120	-0.067
	10	-.111*		0.012	0.000	-0.145	-0.077
	50	-.089*		0.008	0.000	-0.112	-0.066
5	0	.0379*		0.010	0.002	0.010	0.066
	4	0.015		0.009	0.592	-0.012	0.042
	6	-.079*		0.009	0.000	-0.105	-0.053
	10	-.096*		0.011	0.000	-0.129	-0.063
	50	-.074*		0.008	0.000	-0.096	-0.052
6	0	.117*		0.010	0.000	0.089	0.144
	4	.094*		0.009	0.000	0.067	0.120
	5	.079*		0.009	0.000	0.053	0.105
	10	-0.017		0.011	0.654	-0.050	0.016
	50	0.004		0.008	0.992	-0.017	0.026
10	0	.134*		0.012	0.000	0.099	0.169
	4	.111*		0.012	0.000	0.077	0.145
	5	.096*		0.011	0.000	0.063	0.129
	6	0.017		0.011	0.654	-0.016	0.050
	50	0.022		0.010	0.301	-0.008	0.052
50	0	.112*		0.008	0.000	0.088	0.136
	4	.089*		0.008	0.000	0.066	0.112
	5	.074*		0.008	0.000	0.052	0.096
	6	-0.004		0.008	0.992	-0.026	0.017
	10	-0.022		0.010	0.301	-0.052	0.008

In addition to inducing polarity, the pheromone-activated MAPK cascade also leads to changes in gene expression and cell cycle arrest (Fig. 1.2). To determine if the arrest response to pheromone behaves in a similar fashion to polarity establishment, we used the Myo1-yomRuby2 fusion to monitor cell cycle progression following exposure to pheromone (Fig. 3.1D and E, Table 3.4, 3.5 and 3.6). Cells exposed to 4 nM of pheromone spent similar amounts of time in G1 as untreated cells, demonstrating that 4 nM is insufficient to arrest cells. The length of time spent in G1 at 5 nM is significantly different from 4 nM, suggesting that 5 nM is close to the minimum concentration required to arrest cells. The 5 nM concentration also showed the greatest variability in the time spent in G1. We interpret this heterogeneity as further evidence that this concentration is near the transition point. Beyond 5 nM, the length of arrest increased with pheromone concentration. These results are similar to our measurements for polarity establishment.

Table 3.4 Lavene's Test of Homogeneity of Variance for Duration of G1 Stage of the Cell Cycle During Low Pheromone Exposure

Levene Statistic	df1	df2	Sig.
18.734	3	470	.000

Table 3.5 Welch's Analysis of Variance (ANOVA) for Duration of G1 Stage of the Cell Cycle During Low Pheromone Exposure

	Sum of Squares	df	Mean Square	F	Sig.
Between Groups	1617631.081	3	539210.360	174.847	.000
Within Groups	1449431.208	470	3083.896		
Total	3067062.289	473			

Table 3.6 Games-Howell Test of Multiple Comparisons for Duration of G1 Stage of the Cell Cycle During Low Pheromone Exposure

Pheromone Concentration (nM)		Mean Difference (I-J)	Std. Error	Sig.	95% Confidence Interval	
I	J				Lower Bound	Upper Bound
0	4	-8.419	5.100	.353	-21.63	4.80
	5	-51.210[*]	6.113	.000	-67.06	-35.36
	6	-147.623[*]	7.432	.000	-166.93	-128.32
4	0	8.419	5.100	.353	-4.80	21.63
	5	-42.791[*]	6.938	.000	-60.75	-24.83
	6	-139.204[*]	8.124	.000	-160.25	-118.15
5	0	51.210[*]	6.113	.000	35.36	67.06
	4	42.791[*]	6.938	.000	24.83	60.75
	6	-96.413[*]	8.795	.000	-119.18	-73.65
6	0	147.623[*]	7.432	.000	128.32	166.93
	4	139.204[*]	8.124	.000	118.15	160.25
	5	96.413[*]	8.795	.000	73.65	119.18

The polarity network is bistable

Next, we sought to determine the pheromone concentration at which polarized cells no longer maintain polarity (Fig. 3.2 A and B). To ensure all cells started in a polarized state, we exposed cells to a pheromone concentration of 50 nM for two hours. We then lowered the concentration to 10 nM, a sufficiently high concentration to ensure all cells maintain polarity. Following this reduction in pheromone, we lowered the concentration by 1 nM every 15 minutes. Surprisingly, most cells continued to hold polarity and cell cycle arrest at concentrations below the minimum pheromone concentration required for naïve cells to establish polarity (Figs. 3.2 A-C). In fact, a fraction of cells (~30%) held polarity and cell cycle arrest even after pheromone was completely removed. Some of these cells established a second polarity site and began to

44

form a second shmoo. Cells that reentered the cell cycle during the experiment, budded from the

pheromone-induced polarity site without ever losing polarity. The difference between the

minimum pheromone concentration required to establish polarity (~ 6 nM), and the minimum

pheromone concentration required to maintain polarity (~ 0 nM), suggests that the polarity

process is bistable. In terms of a dose-response curve this outcome means that at low pheromone

concentrations there are two stable steady states (unpolarized and polarized) dependent on the

prior history of the cell's exposure (Fig. 1.1). Specifically, cells that have not experienced

pheromone are in the unpolarized state. At pheromone concentrations > 6 nM, the positive

feedback between Cdc42 and the Bem1-Cdc24 complex shifts all cells to a polarized state. Once

polarity is established, the positive feedback is sufficient to maintain polarity even as pheromone

is removed. Establishing the pheromone concentration at which cells resume the cell cycle in this

experiment is challenging (Fig. 3.2C), since the 15-minute steps taken might be shorter than the

time it takes for Myo1 to accumulate in the budding site.
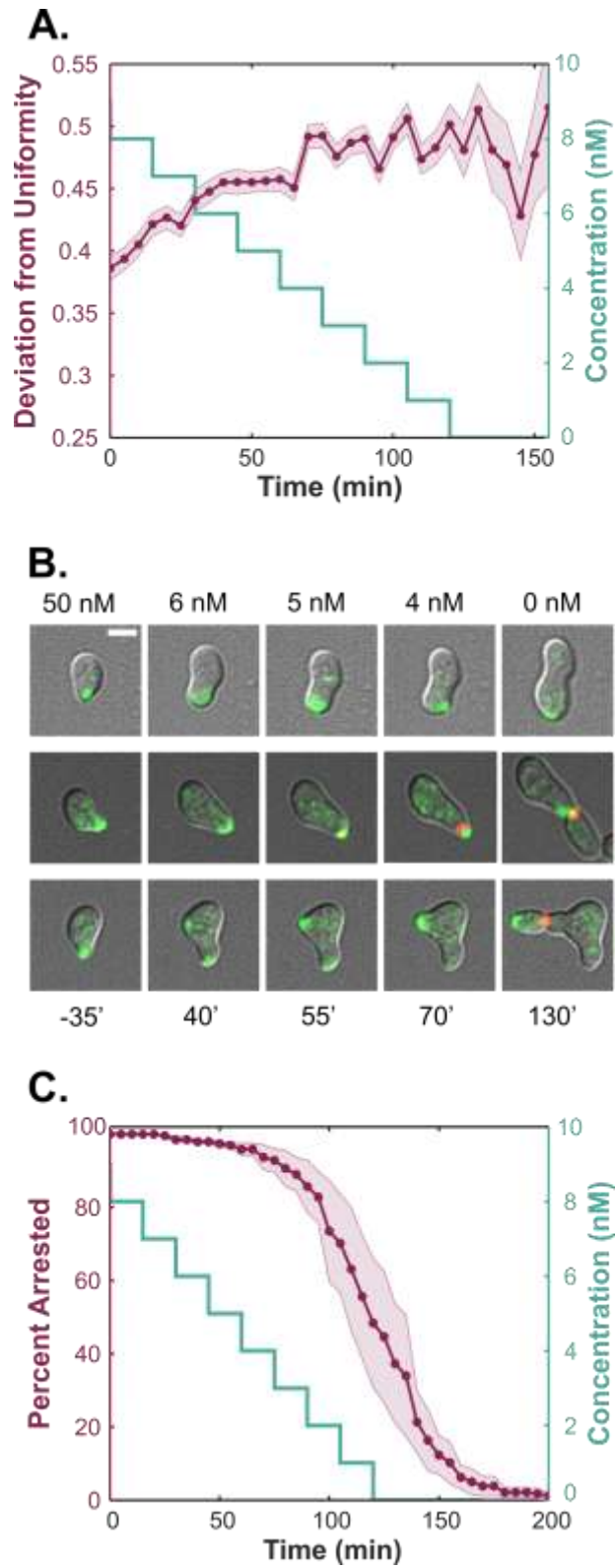
Fig. 3.2 Polarized Cells Maintain Polarity During Multi-Step Pheromone Withdrawal. Cells were exposed to 50 nM pheromone for two hours in order to establish polarity, followed by a reduction of pheromone concentration to 10 nM. Pheromone concentration was then further

reduced by 1 nM every 15 min. **(A)** Mean +/- standard deviation of Bem1-yomNeonGrean deviation from uniformity for G1 cells. Cells maintain polarity throughout the experiment, even in the absence of pheromone. **(B)** Cells show diverse phenotypes during multi-step pheromone reduction. The top cell remains in the G1 stage of the cell cycle and maintains polarity even in the absence of pheromone. The middle cell resumes the cell cycle during the experiment and buds from the original pheromone-induced polarity site. The bottom cell forms a second polarity site leading to a second mating projection before returning to the cell cycle and budding from the second mating projection's polarity site. This cell has two pheromone-regulated polarity sites for a period of time while establishing the second projection. **(C)** The mean percentage +/- standard error of cells remaining in G1 stage of the cell cycle over time. 30% of the cell population is still in G1 30 minutes after pheromone withdrawal to a concentration of 0 nM.

The polarity patch is rapidly disassembled following single-step reductions in pheromone

Since a slow decrease in pheromone concentration revealed hysteresis, we wondered if the rate of pheromone removal affects maintenance of the polarity patch. To test this possibility, we exposed cells to 50 nM pheromone for two hours, then lowered the concentration in one step to either 0 nM, 4 nM, 5 nM or 6 nM pheromone (Fig. 3.3A and B), Interestingly, the polarity patch was not maintained after reduction to a final pheromone concentration of 5 nM or less, but was rapidly disassembled within 5 min. However, the patch remained stable after a reduction to a final concentration of 6 nM. These results are surprising, considering cells maintained polarity after a multi-step reduction to lower pheromone concentrations. The rapid disassembly of the polarity patch suggests the presence of negative regulation that remains active after pheromone removal and disrupts the positive feedback loop required for polarization (Fig. 3.5A). The finding that the number of steps taken to reduce the pheromone concentration determines whether cells maintain polarity is consistent with negative regulation that acts on a different time scale than the positive feedback.

When pheromone is reduced in one step, we posit that the positive feedback loop is rapidly lost in response to the change, while the negative feedback loop adjusts slowly. The persistence of net negative regulation results in the disassembly of the polarity patch. However, when pheromone is reduced slowly, we infer that positive and negative regulation remain balanced so that polarity is maintained. Interestingly, after a reduction to 5 nM pheromone, cells that lost polarity re-established it at the same site after 25-45 min. Polarity re-establishment at the same site suggests that some remnant of the polarity patch remains and is sufficient to reseed polarity once the negative regulation has been sufficiently reduced.

48
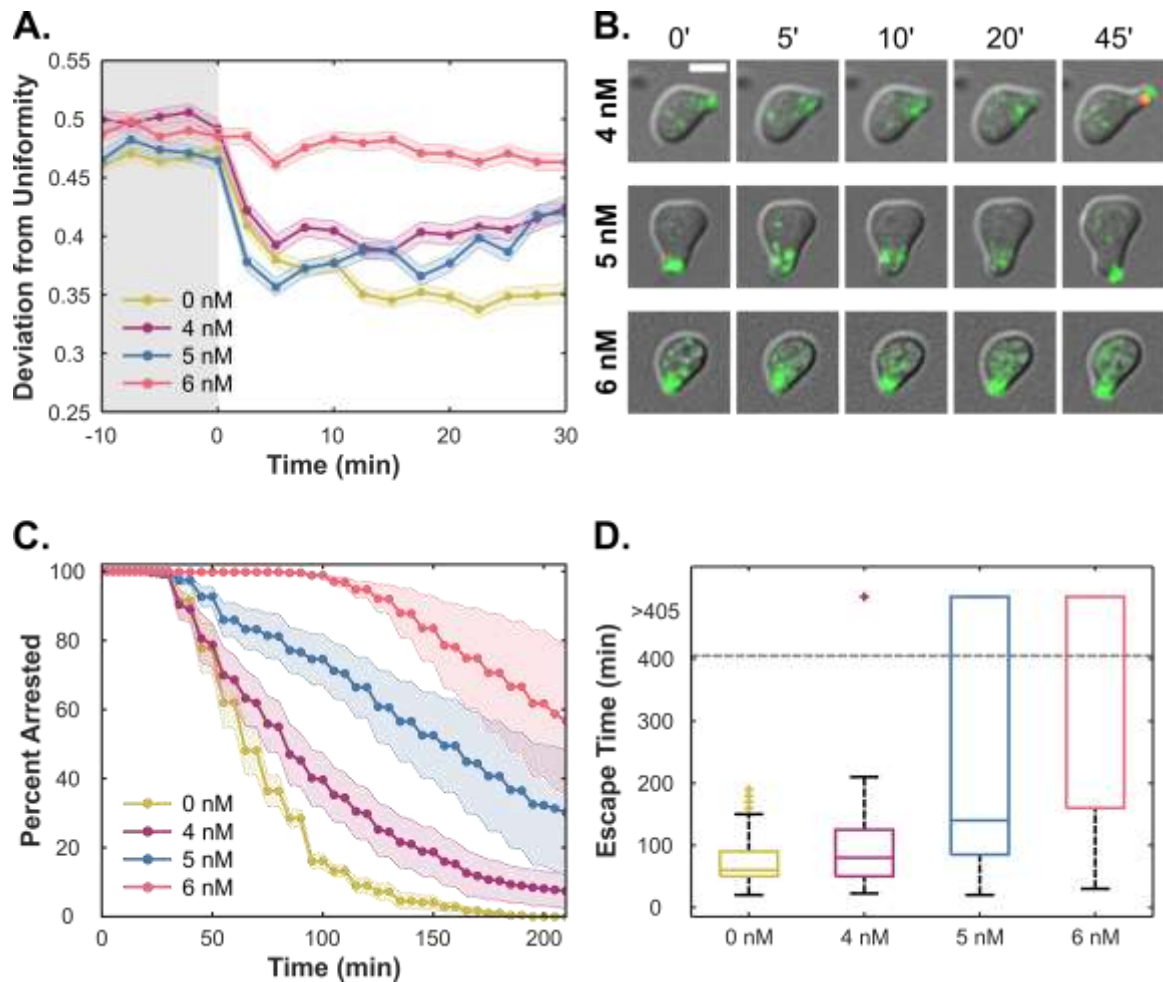
Fig. 3.3 Cells Rapidly Disassembles Polarity Upon One-Step Pheromone Reduction. Cells were exposed to 50 nM pheromone for two hours to establish polarity, followed by a one-step reduction of pheromone concentration to either 0 nM, 4 nM, 5 nM or 6 nM. **(A)** Time traces for mean +/-standard deviation of Bem1-yomNeonGreen deviation from uniformity. Cells rapidly disassemble polarity after a one-step reduction to a pheromone concentration of 5 nM or less but maintain polarity after reduction to 6 nM. **(B)** Representative cells for the 4 nM, 5 nM and 6 nM experiments. **(C)** The mean percentage +/- standard error of cells remaining in G1 stage of the cell cycle after pheromone reduction. Cells remain arrested for longer in the presence of pheromone concentrations lower than those needed to arrest naïve cells. Arrest duration increases with pheromone concentration. **(E)** The distribution of lengths of time cells stay in the G1 stage of the cell cycle after pheromone reduction. Experiment duration is 405 min, and the arrest duration of cells still arrested after the last time point are depicted here qualitatively. Conventions in D are the same as specified in the legend to Fig. 3.1.

In contrast to loss of polarity, only a small amount of pheromone is sufficient to extend duration of cell cycle arrest (Fig. 3.3C and D). The length of cell cycle arrest after a reduction to 0 nM is statistically different from a reduction to all other doses tested (Fig. 3.3D). The observation that exposure to 4 nM pheromone is sufficient to hold arrest after exposure to high pheromone, while naïve cells fail to arrest at the same concentration, suggests that cell cycle arrest is also bistable. The duration of the arrest increases significantly in a dose-dependent manner after a threshold of 4 nM is crossed.

Table 3.7 Lavene's Test of Homogeneity of Variance for Duration of G1 Stage of the Cell Cycle After a One-Step Pheromone Concentration Reduction

Levene Statistic	df1	df2	Sig.
217.740	4	2638	.000

Table 3.8 Welch's Analysis of Variance (ANOVA) for Duration of G1 Stage of the Cell Cycle After a One-Step Pheromone Concentration Reduction

|	Sum of Squares	df	Mean Square	F	Sig.
Between Groups	15706009.426	4	3926502.357	351.990	.000
Within Groups	29427331.663	2638	11155.167		
Total	45133341.090	2642			

Table 3.9 Games-Howell Test of Multiple Comparisons for Duration of G1 Stage of the Cell Cycle After a One-Step Pheromone Concentration Reduction

Pheromone Concentration (nM)		Mean Difference (I-J)	Std. Error	Sig.	95% Confidence Interval	
(I) V	(J) V1				Lower Bound	Upper Bound
0	3	-45.9917*	4.9731	.000	-59.589	-32.395
	4	-32.4317*	4.7430	.000	-45.394	-19.469
	5	-112.0349*	6.6803	.000	-130.309	-93.761
	6	-215.6343*	6.1720	.000	-232.513	-198.756
3	0	45.9917*	4.9731	.000	32.395	59.589
	4	13.5600	5.8927	.145	-2.543	29.663
	5	-66.0433*	7.5402	.000	-86.655	-45.432
	6	-169.6427*	7.0938	.000	-189.030	-150.255
4	0	32.4317*	4.7430	.000	19.469	45.394
	3	-13.5600	5.8927	.145	-29.663	2.543
	5	-79.6033*	7.3905	.000	-99.806	-59.401
	6	-183.2027*	6.9344	.000	-202.154	-164.251
5	0	112.0349*	6.6803	.000	93.761	130.309
	3	66.0433*	7.5402	.000	45.432	86.655
	4	79.6033*	7.3905	.000	59.401	99.806
	6	-103.5994*	8.3796	.000	-126.499	-80.700
6	0	215.6343*	6.1720	.000	198.756	232.513
	3	169.6427*	7.0938	.000	150.255	189.030
	4	183.2027*	6.9344	.000	164.251	202.154
	5	103.5994*	8.3796	.000	80.700	126.499

The rapid disassembly rate of the polarity patch (less than 5 min) was surprising for a system containing positive feedback, where the positive feedback would be expected to maintain polarity for an amount of time after pheromone reduction. To eliminate the possibility that the yomNeonGreen tag on Bem1 is somehow destabilizing the polarity patch and expediting disassembly, we repeated the experiment in a strain that does not contain this tag. Instead, the

strain utilizes a sensor based on the protein binding domain of the Cdc42 effector Gic2 tagged

with a tdTomato fluorescent tag (Fig. 3.4) to image polarity. The strain exhibited the same fast

polarity disassembly dynamics upon pheromone withdrawal observed previously, confirming

that this observation is due to a real biological mechanism.
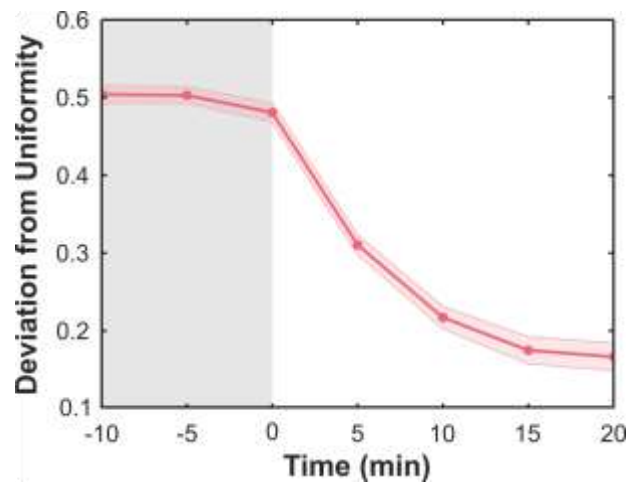
Fig. 3.4 Rapid Polarity Disassembly Upon Pheromone Withdrawal is Not Due to Fluorescent Tag Disruption. Cells containing Gic2PBD-tdTomato as the only fluorescently labeled protein were treated with 50 nM pheromone for 160 min before pheromone concentration was reduced to 0 nM. Deviation from Uniformity of the Gic2PBD-tdTomato distribution showed the same rapid polarity disassembly, confirming this is a real biological phenomenon.

Polarity patch disassembly depends on initial pheromone concentration

Finally, we wanted to test our suggested model of delayed negative regulation (Fig. 3.5). Such a model will predict that the rate at which cells lose polarity after a one-step pheromone reduction will depend on the initial pheromone concentration. A higher initial concentration will result in stronger negative regulation, and therefore a faster disassembly rate. To test this prediction, cells were exposed to either 50 nM pheromone for 120 minutes or 10 nM pheromone for 160 minutes before pheromone was completely withdrawn (Fig. 3.5B). As predicted, the cells exposed to 50 nM pheromone lose polarity at a faster rate than the cells exposed to 10 nM pheromone. Surprisingly, cells exposed to 50 nM pheromone hold cell cycle arrest for longer than cells exposed to 10 nM (Fig. 3.5C). In both concentrations cells resume the cell cycle rather uniformly, but the delay before return to the cell cycle is longer for cells exposed to higher pheromone concentration. That is, the pheromone concentration prior to withdrawal affects persistence of polarity and cell cycle arrest in opposite directions. Higher levels of pheromone increase the duration of cell cycle arrest time but decrease the stability of the polarity patch. These results support the delayed negative regulation model and also suggest that the negative regulation responsible for polarity disassembly is specific to polarity establishment and does not affect the pheromone response pathway as a whole.

Another prediction based on a delayed-negative regulation model is that cells will maintain polarity after a one-step pheromone reduction if the initial pheromone concentration is sufficiently low. A low initial pheromone concentration will result in weak negative regulation that might not be strong enough to disassemble the patch after a reduction in pheromone concentration. To test this prediction, we exposed cells to either 50 nM for 2 hrs. or 10 nM for 160 minutes, and then reduced the pheromone concentration to 5 nM (Fig. 3.5D). As predicted

by the model, cells initially exposed to 50 nM lost polarity rapidly, while cells exposed to 10 nM held polarity. These results show that the disassembly of a polarity patch after pheromone reduction depends on the initial concentration, and again supports a model of slowly-adjusting negative regulation.
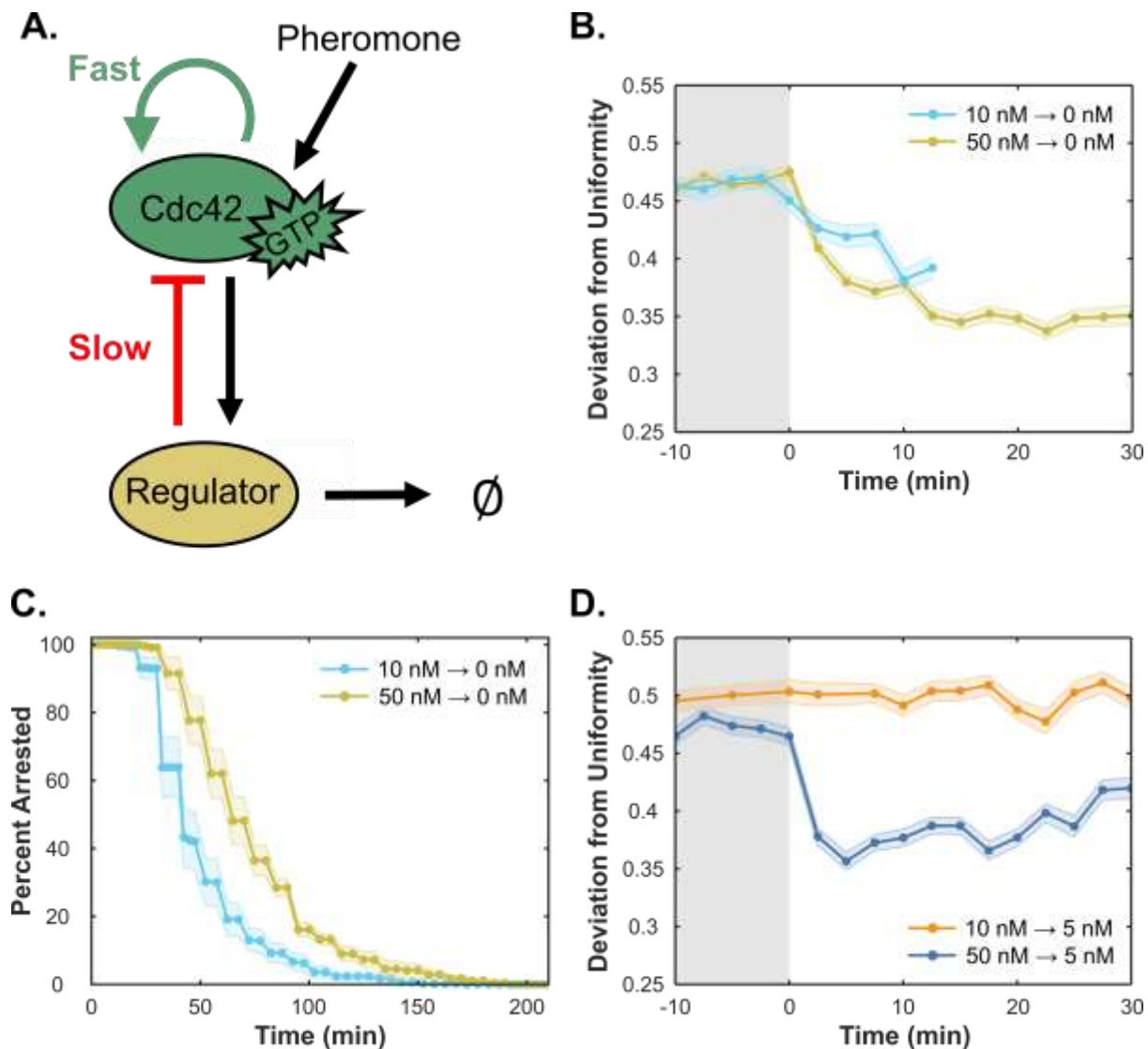
Fig. 3.5 A Model of Slow-Adjusting Negative Regulation and Fast-Adjusting Positive Feedback Successfully Predicts the Influence of Initial Pheromone Concentration on Polarity Disassembly Dynamics After Pheromone Reduction. (**A**) Diagram of the suggested slow-adjusting negative regulation and fast-adjusting positive feedback model. (**B-C**) Cells were exposed to either 50 nM pheromone for two hours or 10 nM for 160 min, followed by a one-step withdrawal of pheromone to 0 nM. (**B**) Time traces for mean +/-standard deviation of Bem1-yomNeonGreen deviation from uniformity. Cells exposed initially to 10 nM pheromone lose polarity at a slower rate than those initially exposed to 50 nM. (**C**) The mean percentage +/-standard error of cells remaining in G1 stage of the cell cycle after pheromone withdrawal. Cells exposed to 10 nM initially resume cell cycle faster than those initially exposed to 50 nM, suggesting the initial pheromone concentration affects polarity and cell cycle arrest in opposite directions. (**D**) Cells were exposed to either 50 nM pheromone for two hours or 10 nM for 160 min, followed by a one-step reduction of pheromone to 5 nM. Cells exposed initially to 10 nM pheromone maintain polarity after the reduction while cells exposed to 50 nM initially do not.

56

Bem3 is a Possible Mechanism for Negative Regulation of Polarity Upon Pheromone Withdrawal

We were interested in identifying the molecular mechanism facilitating the polarity patch disassembly upon one-step pheromone withdrawal. One possible mechanism are GAPs that could be either transcribed in a pheromone dependent manner, creating an incoherent feedforward loop, or recruited by Cdc42 or its effectors to the polarity patch, creating a negative feedback loop. Budding yeast has three Cdc42 GAPs – Bem3, Rga1 and Rga2 (Bender & Pringle, 1991; Madden & Snyder, 1998; G. R. Smith et al., 2002; Stevenson et al., 1995; Zheng et al., 1993). Another possible mechanism is Cdc42 mediated recruitment of a kinase that in turn phosphorylates the GEF Cdc24, reducing its activity and targeting it for destruction. Budding yeast has three such kinases, Ste20, Skm1 and Cla4 (Frieser, Hlubek, Sandrock, & Bölker, 2011b; M. P. Gulli et al., 2000).

To investigates Bem3 as a possible negative feedback mechanism, mutant strains lacking *BEM3* were exposed to 50 nM of pheromone for 2 hours, followed by a withdrawal to a pheromone concentration of 0 nM (Fig. 3.6). The images do show what seems to be a slight lingering of the polarity patch, but further quantification of the data will be needed to determine whether or not this observation holds true. Additionally, mutant cells displayed several strange phenomena, such as Myo1 localization to the shmoo tip during polarity disassembly while cells were still at the G1 stage of the cell cycle. Wild-type cells do not show any Myo1 localization during polarity patch disassembly. Myo1 is only visible in wild-type cells while cells are not in the G1 stage of the cell cycle, which occurs at a much later time point following pheromone withdrawal. Additionally, while wild-type cells usually bud from the pheromone-regulated polarity site following a pheromone withdrawal, the *bem3Δ* mutants repolarize and bud from a different site.
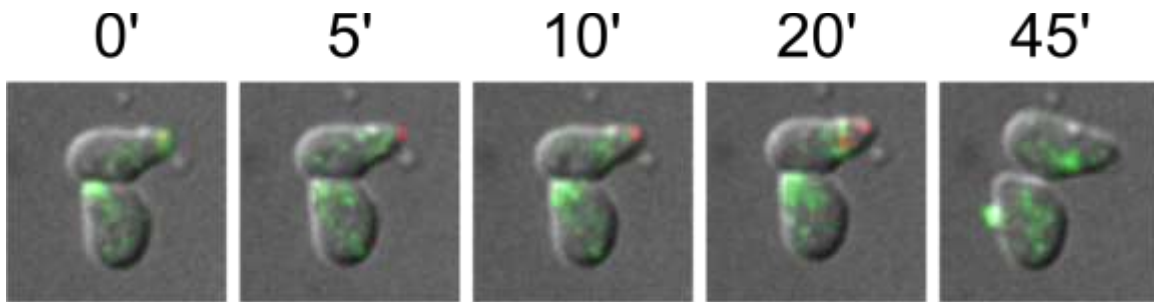
Figure 3.6 Bem3 Might Contribute to Negative Regulation of Polarity Upon One-Step Pheromone Withdrawal. *bem3Δ* cells exposed to 50 nM pheromone for 2 hrs. followed by a pheromone withdrawal show a lingering polarity patch, localization of My01 at the shmoo tip and budding from a place other than the pheromone-regulated polarity patch.

Negative Regulators Might Play a Role in Early Polarity Establishment and Wandering

We were also interested in whether a negative regulatory mechanism such as Cdc42 GAPs and Cdc24 phosphorylation can play a role in early polarity patch establishment and wandering towards a potential gradient. We therefore studied polarity establishment in cells lacking one of the GAPs or featuring a Cdc24 mutant where all phosphorylation sites were mutated to alanine residues. We exposed these strains to 50 nM pheromone and watched polarity patch formation and wandering.

All mutants seem to establish polarity at roughly the same rate, with the exception of the *bem3Δ* strain, which might polarize slightly quicker. Potential differences in the rate of polarity establishment between the mutants are likely quantitative, and further analysis will be needed to determine whether such differences are significant. Strikingly, the *rga1Δ* strain seems to display a much broader polarity patch that wanders back and forth. This phenotype was present on a population level for this mutant, suggesting that Rga1 might play a role as a negative regulator that restricts patch width and mobility.
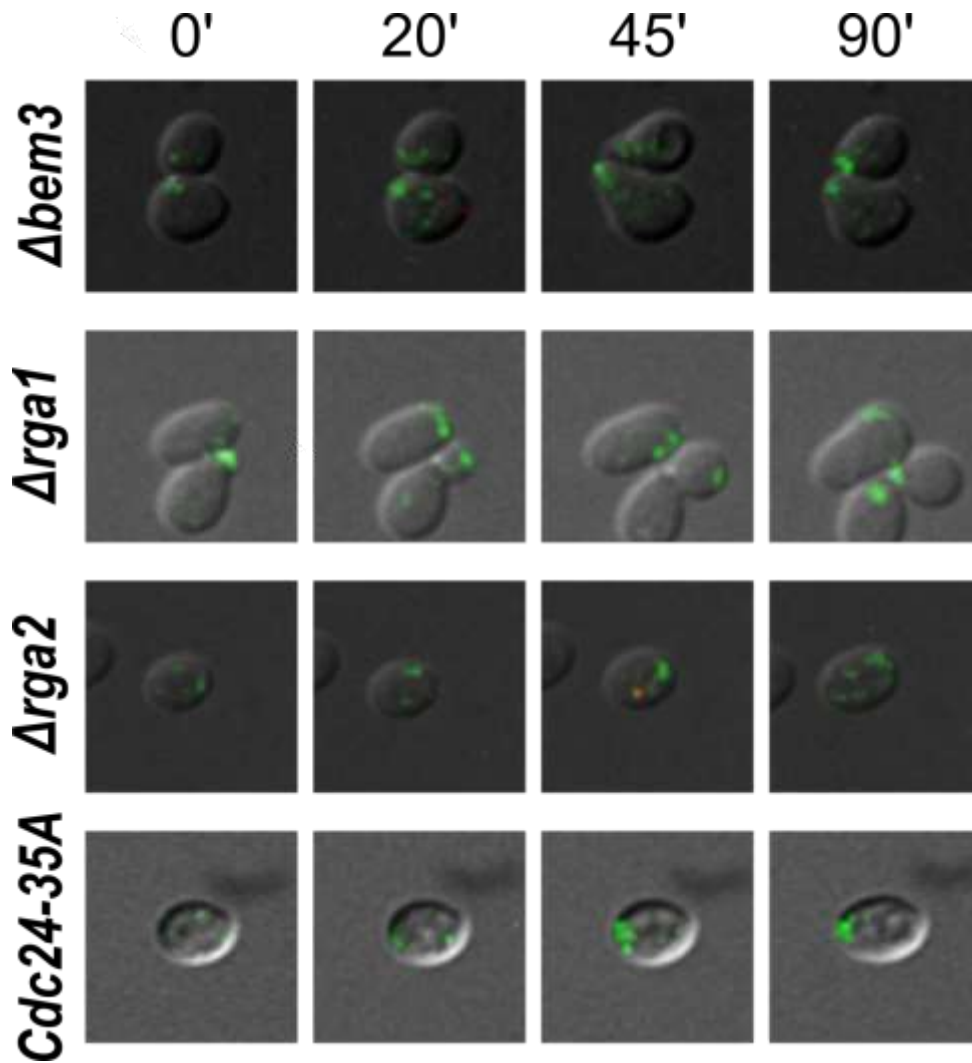
Fig. 3.7 The Role of Negative Regulators in Early Polarity Establishment and Wandering. Mutant cells either lacking a GAP or containing unphosphorylatable Cdc24 were exposed to 50 nM pheromone and imaged for Bem1-yomNeonGreen. All mutants seem to establish polarity at roughly the same rate, with the exception of the *bem3Δ* strain, which might polarize slightly quicker. Strikingly, the *rga1Δ* strain seems to display a much broader polarity patch that wanders back and forth.

CHAPTER 4 - DISCUSSION

Differences in Polarity Establishment Rates Could Help Cells Avoid Polarizing in the Wrong Direction

A question of current interest in cell biology is how symmetry breaking occurs during morphogenesis. Budding yeast represent an ideal model system for addressing this question. Yeast cells are able to polarize their growth in response to extracellular pheromone concentrations in the absence of internal or external spatial cues using purely biochemical interactions. Various models have been proposed for how this symmetry breaking occurs (Goryachev & Pokhilko, 2008; Howell et al., 2009, 2012; Marco et al., 2007). All these models involve a positive feedback loop to amplify local regions of signaling activity. A standard way to characterize non-linear systems that feature a positive feedback is to systematically vary stimulus while measuring a response and look for stimulus concentrations or transitions points in which the response significantly changes. For pheromone-regulated polarity, we sought to determine the pheromone concentration at which cells transition from an unpolarized to a polarized state. Our experiments revealed that this transition or bifurcation point occurs at a pheromone concentration of ~6 nM. This value is close to the reported value of the Kd for the receptor (Reneke et al., 1988).

While cells establish polarity in all pheromone concentrations of 6 nM or higher, our analysis also revealed a significant variation in the time required to polarize that is a function of the stimulus concentration. At 10 nM cells took less than 40 min to polarize, whereas at 6 nM the time to polarize took approximately 100 min. A change in the response time scale is also a

characteristic of systems near a bifurcation point and provides further evidence that 6 nM is close

to the transition from an unpolarized to a polarized state. The variation in the time to polarize

might also have a biological function. A low pheromone concentration might indicate a mating

partner is further away. Slow polarity establishment might be advantageous in this case in order

to allow the cell to accurately detect the direction of the gradient and to employ gradient

detection methods such as time averaging. In contrast, a high pheromone concentration might

indicate that a mating partner is nearby and a mating attempt might be successful even without

an accurate gradient detection. Under such conditions, an estimation of the gradient direction

might be sufficient and a cell might prefer to polarize quickly in order to claim its mating partner

first.

Bistability Might Enable Cells to Filter Out Fluctuation and Only Respond to Significant Changes in Pheromone Concentration

In addition to promoting polarization, positive feedback can also generate bistability. In

the context of polarity establishment, bistability means that for a range of pheromone

concentrations both the spatially homogenous and polarized distributions of Cdc42 are stable and

the distribution that is observed depends on the history of the system. Establishing whether or

not the polarity circuit is bistable is important for understanding both the molecular mechanisms

that drive polarization and the design principles that allow yeast to reliably detect and grow

toward potential mating partners. In particular, determining whether polarity is bistable can

confirm or deny a class of mathematical models. Some mathematical models for polarity

establishment are inherently bistable, like wave-pinning (Mori et al., 2008; Semplice et al.,

2012), while others, like Turing models, can be either bistable or monostable (Goryachev &

Pokhilko, 2008; Howell et al., 2012; Savage et al., 2012). For bistable wave pinning models, the

spatially homogenous steady state remains stable and a perturbation of finite size is required to

drive the systems to the polarized state. The long delay in polarity establishment seen at 6 nM is consistent with the system being bistable and near the bifurcation point, requiring a long time for a finite fluctuation of active Cdc42 to initiate the positive feedback loop that drives polarity establishment. To firmly establish the presence of bistability, we designed and conducted experiments to test for hysteresis in the polarity response. We prepared cells in a polarized state and then systematically reduced the pheromone concentration in either a single step or a multi-step manner. Using this approach, we found a significant population of cells that held polarity even after pheromone was completely removed in a multi-step manner. In contrast, cells lost polarity when pheromone was reduced in one step to a concentration of 5 nM or less. Cells can exist in two steady states, either polarized or unpolarized, after a reduction in pheromone concentration, clearly demonstrating the existence of hysteresis and bistability in the polarity circuit.

One benefit of relying on a bistable mechanism is the suppression of polarity establishment driven by weak signals. Yeast undergo morphological changes in order to reach a potential mate. This process is energetically costly and presumably only undertaken when there is a high probability of successful mating. Building bistability into the system may guard against unproductive mating attempts. Another benefit of a bistable system is establishing robust polarity in the face of small fluctuations in signal strength. The strength of a pheromone gradient will likely fluctuate over time due to stochastic changes in pheromone expression in the secreting cell or temporary changes in the environment. Bistability may enable the cell to filter out these noisy fluctuations in order to successfully mate, and only respond to changes in pheromone concentration if they are deemed significant.

Possible Mechanisms Facilitating Negative Feedback

Our analysis also revealed the existence of a negative feedback loop that acts over a longer time scale than the positive feedback that drives polarity. This negative feedback loop rapidly disrupts the polarity site when pheromone is suddenly removed. While this negative feedback acts in opposition to polarity establishment, its presence may be critical for reorientation of the polarity site when initial polarization is not aligned with the gradient or for rapid dismantling of the polarity site if the gradient changes directions or is removed completely, as would be the case when a competing suitor successfully mates with the pheromone secreting partner.

A previous modeling study of polarity in yeast showed has shown that negative feedback builds robustness against fluctuations in the concentration of polarity components, thus increasing the range of polarity protein concentrations, and possibly pheromone concentration, at which polarization is possible (Howell et al., 2012). The same study showed that models containing a negative feedback loop has smaller region of parameter space in which bistability occurs, and suggests that the size of the bistable region depends on the number of steps leading to the negative feedback (Howell et al., 2012). These observations suggest that the slow-adjusting characteristic of the negative feedback might allow for the existence of bistability in the system.

One possible mechanism for the negative feedback observed in our results is phosphorylation of the GEF Cdc24. It has previously been shown that phosphorylation of the Cdc24 reduces the GEFs activity and targets it for destruction. The PAKs responsible for Cdc24 phosphorylation are all recruited by Cdc42, forming a negative feedback loop (Frieser, Hlubek, Sandrock, & Bölker, 2011a; M.-P. Gulli et al., 2000; Howell et al., 2012; Kozubowski et al.,

2008). However, because this negative feedback loop involves phosphorylation, it is probably too fast to account for our results and is more likely to play a role in ensuring the emergence of a unique polarity site (Howell et al., 2009, 2012). It is likely that the feedback loop that rapidly dismantles the polarity site involves a GAP, or a combination of GAPs. A previous study has shown that a model containing a GAP-mediated feedback loop has a larger bistable region of parameter space compared to a model containing a GEF phosphorylation-mediated feedback loop, further supporting GAPs as the more likely mechanism of negative feedback (Howell et al., 2012). The GAP-mediated feedback loop could due to pheromone-regulated transcription or to the recruitment of the GAPs to the polarity site by Cdc42 or other polarity proteins. Preliminary results from our lab show that the transcription of all three GAPs is regulated in a pheromone dependent manner (data not shown). Additionally, a previous study has shown that at least one of the GAPs, Rga1, localizes to the polarity patch (Tkach et al., 2012).

Lastly, it is also possible that the negative feedback is mediated by vesicle delivery. Vesicles could be diluting polarity factors when merging with the membrane at the polarity site. Moreover, the concentration of Cdc42 in vesicles has been shown to be lower than the concentration of Cdc42 in the polarity site (Watson, Rossi, & Brennwald, 2013). In fact, a previous study has shown that vesicle delivery is a negative feedback mechanism that pushes the polarity patch away from the vesicle delivery site, thus aiding in gradient detection (McClure et al., 2015). The time scale of the negative feedback attenuation after a reduction in pheromone concentration is consistent with the half-life of actin cables (~25 min), suggesting this is a possible mechanism for polarity patch disassembly (Yang & Pon, 2002).

Bistability in Pheromone-Regulated Cell Cycle Arrest

Because the cells used in our experiments contained a cell-cycle marker (Myo1-yomRuby), we were also able to determine the concentration of pheromone required to impose cell cycle arrest. Our findings show that while naïve cells require at least 5 nM to arrest their cell cycle, a lower concentration is sufficient to lengthen cell cycle arrest in already arrested cells. The difference between the pheromone concentration required to arrest cells and that required to lengthen cell cycle arrest suggest that the cell cycle also displays hysteresis and is possibly bistable.

Cell cycle arrest hysteresis has been previously reported, where cells pre-exposed to a high-concentration pheromone pulse followed by a reduction of pheromone concentration remained arrested for longer than naïve control cells exposed to the same final pheromone concentration. The same paper concluded that the source of hysteresis was increased inhibition of the G1 cyclins Cln1 and Cln2 in pheromone-arrested cells due to increased pheromone-dependent transcription of the cell-cycle inhibitor Far1 (Doncic & Skotheim, 2013). Cells exposed to high levels of pheromone have higher Far1 abundance, allowing them to lengthen cell cycle arrest to a greater extent than naïve cells with lower Far1 abundance. The Far1 abundance mechanism described in the Doncic paper is most likely also responsible for the cell cycle hysteresis we also observed.

Additionally, bistability in the mating pathway has also been suggested at the transcriptional level. A previous study has shown that cells exhibit varying levels of Fus1 and Fus3 expression when exposed to pheromone, and that these differences in levels corresponds to whether or not cells were forming mating projections, but not to cell cycle arrest. Fus1 and Fus3 are both pheromone regulated genes and are good indicators of transcription of other proteins

that are pheromone-regulated. The same study employed mathematical modeling to identify the mechanism creating bistability. The model featured the active MAPKs Fus3 and Kss1 as positive regulators of transcription, while the inactive form of Kss1 serves as a negative regulator. Additionally, the model featured the pheromone response specific transcription factor Ste12 as a positive feedback loop that upregulates its own transcription, as well as the transcription of Fus3 and Kss1. The model showed that the role of Kss1 as both a negative and positive regulator, as well as the Ste12 positive feedback are essential for creating transcription-level bistability (Paliwal et al., 2007).

There are some key differences between our study and the Paliwal study. The Paliwal study looked at cells exposed to pheromone for 6 hrs, while our study looked at cells exposed for a much shorter time scale (less than 3 hours). The difference in pheromone exposures might result in different abundance of regulators and pathway dynamics. Additionally, the Paliwal paper correlated differences in transcription level with the ability to form mating projections, but not with cell cycle arrest decisions. Therefore, bistable regulation in transcription is more likely to be connected to bistability in polarity regulation than bistability in the cell cycle.

Differences Between Pheromone-Regulated Polarity and Cell Cycle Arrest

While both pheromone-regulated polarity and cell cycle arrest display hysteresis, they do so in significantly different ways. For polarity, the existence of the two steady states comes from the difference in response to a one-step reduction of pheromone concentration where cells quickly disassemble polarity, versus a multi-step reduction where cells maintain polarity. For cell cycle arrest, the existence of two steady states comes from cells pre-exposed to a high pheromone concentration maintaining arrest in lower pheromone concentrations where naïve cells fail to arrest. Additionally, the strength of pheromone concentration to which cells are

exposed prior to a one-step reduction affects cell cycle arrest and polarity in opposite direction. A lower initial pheromone concentration will increase polarity patch stability after a one-step pheromone concentration reduction, while decreasing the length of cell cycle arrest.

An explanation for these differences is that the negative feedback we identified is acting on the polarity level and not on the cell cycle level. Cells must be able to polarize in the direction of a pheromone gradient. The pheromone gradient experienced by a cell can fluctuate as a result of changes in the environment or changes in pheromone expression in the secreting cell. Additionally, closer potential mating partners could enter the G1stage of the cell cycle and begin secreting pheromone as well, creating a second, much stronger, pheromone cue. Cells must be able to reorient their polarity site in response to any of these changes quickly, and polarity-specific negative regulation can be a mechanism to facilitate these changes. In contrast, cell cycle arrest is not in any way dependent on an accurate detection of the pheromone gradient and does not require fast response mechanisms. Significant changes in pheromone concentrations could indicate the need to adjust gradient detection and reorient the polarity site. Under these conditions, it might be advantageous for cells to disassemble their polarity site in order to reorient it while still maintaining cell cycle arrest. The need for quick polarity adjustment while still maintaining cell cycle arrest might be the biological function of the different hysteresis behaviors observed for pheromone regulated polarity and cell cycle arrest.

Our studies have shown that pheromone regulated polarity in yeast is bistable and exhibits a mechanism of memory. We have also proposed and confirmed a model of slow-adjusting negative regulation and fast-adjusting positive feedback that plays a role in this mechanism of memory. The presence of bistability and hysteresis is pheromone regulated

polarity is informative to the study of polarity networks in other organisms and will inform

future models of polarity establishment.

CHAPTER 5 – FUTURE DIRECTIONS

Additional Experiments for the Study of Pheromone-Regulated Polarity Establishment

The work described in this dissertation brings additional interesting questions that can create new research projects. While our preliminary results indicate Bem3 as the possible negative feedback regulator, additional experiments are needed. Specifically, the preliminary data for all negative feedback mutants must be quantified and compared to quantitative data from the wild-type strain in order to confirm the negative feedback mechanisms. Additional experiments can be done to investigate the mechanism for Myo1 localization during polarity patch disassembly in the *bem3Δ* strain, and to identify mechanisms regulating budding from a site different than the pheromone-regulated polarity site in this mutant. Similarly, the data showing changes in polarity patch mobility in the *rga1Δ* mutant also needs to be quantified and compared to a wild type strain. In order to check for any redundancy or cooperation between negative regulators, similar experiments should be done in strains containing double deletions of GAPs. Lastly, similar experiments can be done in the presence of Latrunculin A (LatA), a toxic natural product that causes disruption of the actin cytoskeleton. A change in the rate of polarity disassembly after a one-step pheromone withdrawal in the presence of LatA will indicate actin-mediated vesicles as a possible mechanism of negative feedback driving polarity patch disassembly.

Experiments can also be done to determine whether the polarity-level negative regulation is a result of a negative feedback motif or an incoherent feedforward loop (Rahi et al., 2017). A

negative feedback loop can be experimentally distinguished from an incoherent feedforward by exposing cells to a high level of pheromone for varying lengths of time before a one-step pheromone withdrawal. In a system with an incoherent feedforward loop, the negative regulator would accumulate over time, resulting in a faster polarity disassembly rate for longer pheromone exposures. In contrast, a negative feedback loop reaches a stable level for a given pheromone concentration that does not change over time. Thus, a lengthened exposure to pheromone before a one-step withdrawal would have no effect on disassembly time. The suggested experiment is a simple way to determine experimentally and conclusively the regulatory motif facilitating polarity disassembly.

The results described in this dissertation can also inform new mathematical modeling efforts. In particular, predictive models featuring a fast-acting positive feedback and a slow-active negative regulation can be used to further validate our findings. Models featuring different negative regulation motifs can also be used to fit our data and determine the most likely negative regulation mechanism. Lastly, quantitative fitting of the data we discussed in this dissertation can be used to distinguish wave-pinning and Turing models and determine the most likely class of models.

Lastly, we have also made an additional observation not described in this dissertation. Cells treated with pheromone in a pulse-like manner establish polarity at a much quicker rate upon second and third pulses than naïve cells exposed to pheromone for the first time. The bistable regulation of polarity could be responsible for this display of memory. Additional experiments and mathematical modeling efforts can determine the contribution of bistability to this faster polarity assembly rate upon second exposure to pheromone.

Consequences of this Work for the Study of Polarity Establishment in Other Organisms

While the work described here was done in budding yeast, our hope is that this work will serve as a template for the study of polarity establishment in higher eukaryotes, including human cells. We designed a series of simple yet elegant experiments to determine whether pheromone-regulated polarity establishment in yeast is a bistable process and have shown that indeed this system exhibits hysteresis and bistability. The same experimental methodology can be employed to test for bistability in human cellular processes featuring polarity regulated by an external cue, such as T-cell's response to pathogens, fibroblast migration toward wound sites, and neuron growth toward nerve growth factor during development (Skupsky et al., 2005). Neutrophils, fibroblasts and neurons can be exposed to varying concentrations of stimulus in a microfluidic chamber to determine the minimum stimulus concentration required to establish polarity. Cells can then be exposed to a high level of stimulus sufficient to establish polarity followed by either a one-step or a multi-step reduction in stimulus concentration in order to determine the minimum concentration required to maintain polarity and test for hysteresis. Experiments in higher eukaryotes will help determine whether bistability is a consensus feature of polarity establishment across pathways and organisms, or whether the number of steady states of polarity changes according to context.

Additionally, a further investigation into the role bistability might play in disease is needed. Several human diseases are connected to changes in polarity regulation. For instance, polarity pathways are often perturbed by oncogenic signaling. Loss of polarity is one of the hallmarks of cancer, causing cancer cells to display alterations of cell shape, cell-cell adhesion, and cell motility. These qualities are likely important for numerous aspects of malignant transformation and play a key role in cancer metastasis (Bardwell, 2004; Iden & Collard, 2008;

M. Lee & Vasioukhin, 2008). A possible mechanism for the alternation of polarity pathways by oncogenic signaling is a change in the number of stable steady states that allow cancer cells to establish or lose polarity more easily. An interesting experiment would include utilizing the experimental strategy we developed to determine bistability in both normal and oncogenic cells to see if an alteration in the number of study states has occurred.

Future Work Related to Pheromone Regulated Cell Cycle Arrest

During our work on this dissertation, we have made additional observations that were not directly connected to the topic of this dissertation but could lead to additional interesting research projects. One such observation is that cells that are not at the G1 stage of the cell cycle can form a much more stable polarity patch once they arrest their cell cycle than cells who are initially at the G1 stage of the cell cycle. A possible mechanism for this difference can be pheromone-induced transcription of polarity proteins while cells finish their cell cycle. Pheromone induced transcription can be measured using a fluorescent reporter regulated by a pheromone-induced transcription motif, such as the Fus1 promoter. The level of the reporter could be quantified and correlated to polarity patch stability.

We have also observed that exposure to high pheromone concentrations followed by a one-step reduction to a lower pheromone concentration leads to polarity site reorientation and turning. This experimental design can be used to easily investigate and identify molecular mechanisms regulating gradient detection and turn formation. For example, this experimental strategy can be done in strains containing fluorescently labeled septins to study the regulation of septin deposition in the context of gradient detection.

We have also observed that daughter cells are much more likely to respond to pheromone than mother cells. A higher percentage of daughter cells arrest their cell cycle and/or forms much

more stable polarity patches at low pheromone concentrations. Possible mechanisms creating this difference between mother and daughter cells can be daughter-specific transcription or an uneven segregation of proteins, such as Far1 (Doncic et al., 2015). An experiment in which levels of fluorescently labeled Far1 are correlated with cell cycle arrest and polarity in mother and daughter cells can confirm or refute Far1 segregation as a possible mechanism responsible for mother-daughter differences in pheromone response. Additionally, experiments done in cells with a deletion of the daughter-specific, pheromone response pathway related transcription factor Dse1can expose or refute another potential mechanism regulating differences between mother and daughter cells.

Lastly, we noticed septin localization defects in cells lacking the G1 cyclin Cln3, suggesting that Cln3 plays a role in septin regulation. An experiment correlating Cln3 levels with the localization of fluorescently labeled septins can expose an important mechanism of cell cycle dependent septin regulation.

REFERENCES

Adams, A. E. M., Johnson, D. I., Longnecker, R. M., Sloat, B. F., & Pringle, J. R. (1990). CDC42 and CDC43, two additional genes involved in budding and the establishment of cell polarity in the yeast Saccharomyces cerevisiae. *Journal of Cell Biology*, *111*(1), 131–142. http://doi.org/10.1083/jcb.111.1.131

Alani, E., Cao, L., & Kleckner, N. (1987). A Method for Gene Disruption That Allows Repeated Use of, *1*(Miller 1972), 0–4. http://doi.org/10.1534/genetics.112.541.test

Arkowitz, R. a. (2009). Chemical gradients and chemotropism in yeast. *Cold Spring Harbor Perspectives in Biology*, *1*(2), a001958. http://doi.org/10.1101/cshperspect.a001958

Bardwell, L. (2004). A walk-through of the yeast mating pheromone response pathway. *Peptides*, *25*(9), 1465–76. http://doi.org/10.1016/j.peptides.2003.10.022

Barkai, N., Rose, M. D., & Wingreen, N. S. (1998, December). Protease helps yeast find mating partners. *Nature*. England. http://doi.org/10.1038/24760

Bender, A., & Pringle, J. R. (1991). Use of a screen for synthetic lethal and multicopy suppressee mutants to identify two new genes involved in morphogenesis in Saccharomyces cerevisiae. *Molecular and Cellular Biology*, *11*(3), 1295–1305.

Boeke, J. D., LaCroute, F., & Fink, G. R. (1984). A positive selection for mutants lacking orotidine- 5'-phosphate decarboxylase activity in yeast: 5-fluoro-orotic acid resistance. *Mol Gen Genet*, *197*(2), 345–6.

Bose, I., Irazoqui, J. E., Moskow, J. J., Bardes, E. S., Zyla, T. R., & Lew, D. J. (2001). Assembly of scaffold-mediated complexes containing Cdc42p, the exchange factor Cdc24p, and the effector Cla4p required for cell cycle-regulated phosphorylation of Cdc24p. *The Journal of Biological Chemistry*, *276*(10), 7176–86. http://doi.org/10.1074/jbc.M010546200

Brachmann, C. B., Davies, A., Cost, G. J., Caputo, E., Li, J., Hieter, P., & Boeke, J. D. (1998). Designer deletion strains derived from Saccharomyces cerevisiae S288C: A useful set of strains and plasmids for PCR-mediated gene disruption and other applications. *Yeast*, *14*(2), 115–132. http://doi.org/10.1002/(SICI)1097-0061(19980130)14:2<115::AID-YEA204>3.0.CO;2-2

Bradham, C., & McClay, D. R. (2006). p38 MAPK in development and cancer. *Cell Cycle (Georgetown, Tex.)*, *5*(8), 824–828. http://doi.org/10.4161/cc.5.8.2685

Causin, P., & Facchetti, G. (2009). Autocatalytic loop, amplification and diffusion: a mathematical and computational model of cell polarization in neural chemotaxis. *PLoS Computational Biology*, *5*(8), e1000479. http://doi.org/10.1371/journal.pcbi.1000479

Chen, G., Deng, C., & Li, Y.-P. (2012). TGF-beta and BMP signaling in osteoblast differentiation and bone formation. *International Journal of Biological Sciences*, *8*(2), 272–288. http://doi.org/10.7150/ijbs.2929

Chou, C.-S., Nie, Q., & Yi, T.-M. (2008). Modeling robustness tradeoffs in yeast cell polarization induced by spatial gradients. *PloS One*, *3*(9), e3103. http://doi.org/10.1371/journal.pone.0003103

Ciejek, E., & Thorner, J. (1979). Recovery of S. cerevisiae a cells from G1 arrest by alpha factor pheromone requires endopeptidase action. *Cell*, *18*(3), 623–635.

Doncic, A., Atay, O., Valk, E., Grande, A., Bush, A., Vasen, G., … Skotheim, J. M. (2015). Compartmentalization of a bistable switch enables memory to cross a feedback-driven transition. *Cell*, *160*(6), 1182–1195. http://doi.org/10.1016/j.cell.2015.02.032

Doncic, A., & Skotheim, J. M. (2013). Feedforward regulation ensures stability and rapid reversibility of a cellular state. *Molecular Cell*, *50*(6), 856–68. http://doi.org/10.1016/j.molcel.2013.04.014

Dyer, J., Savage, N., Jin, M., & Zyla, T. (2013). Tracking shallow chemical gradients by actin-driven wandering of the polarization site. *Current Biology*, *23*(1), 32–41. http://doi.org/10.1016/j.cub.2012.11.014.Tracking

Ferrell, J. E. (2002). Self-perpetuating states in signal transduction: positive feedback, double-negative feedback and bistability. *Current Opinion in Cell Biology*, *14*(2), 140–148. http://doi.org/10.1016/S0955-0674(02)00314-9

Ferrell, J. E., & Xiong, W. (2001). Bistability in cell signaling: How to make continuous processes discontinuous, and reversible processes irreversible. *Chaos (Woodbury, N.Y.)*, *11*(1), 227–236. http://doi.org/10.1063/1.1349894

76

Ferry, M. S., Razinkov, I. A., & Hasty, J. (2011). *Microfluidics for Synthetic Biology. Synthetic Biology, Part A* (1st ed., Vol. 497). Elsevier Inc. http://doi.org/10.1016/B978-0-12-385075-1.00014-7

Frieser, S. H., Hlubek, A., Sandrock, B., & Bölker, M. (2011a). Cla4 kinase triggers destruction of the Rac1-GEF Cdc24 during polarized growth in Ustilago maydis. *Molecular Biology of the Cell*, *22*(17), 3253–3262. http://doi.org/10.1091/mbc.E11-04-0314

Frieser, S. H., Hlubek, A., Sandrock, B., & Bölker, M. (2011b). Cla4 kinase triggers destruction of the Rac1-GEF Cdc24 during polarized growth in Ustilago maydis. *Molecular Biology of the Cell*, *22*(17), 3253–62. http://doi.org/10.1091/mbc.E11-04-0314

Geest, C. R., & Coffer, P. J. (2009). MAPK signaling pathways in the regulation of hematopoiesis. *Journal of Leukocyte Biology*, *86*(2), 237–250. http://doi.org/10.1189/jlb.0209097

Goryachev, A. B., & Pokhilko, A. V. (2008). Dynamics of Cdc42 network embodies a Turing-type mechanism of yeast cell polarity. *FEBS Letters*, *582*(10), 1437–1443. http://doi.org/10.1016/j.febslet.2008.03.029

Gulli, M.-P., Jaquenoud, M., Shimada, Y., Niederhäuser, G., Wiget, P., & Peter, M. (2000). Phosphorylation of the Cdc42 Exchange Factor Cdc24 by the PAK-like Kinase Cla4 May Regulate Polarized Growth in Yeast. *Molecular Cell*, *6*(5), 1155–1167. http://doi.org/https://doi.org/10.1016/S1097-2765(00)00113-1

Gulli, M. P., Jaquenoud, M., Shimada, Y., Niederhäuser, G., Wiget, P., & Peter, M. (2000). Phosphorylation of the Cdc42 exchange factor Cdc24 by the PAK-like kinase Cla4 may regulate polarized growth in yeast. *Molecular Cell*, *6*(5), 1155–67. Retrieved from http://www.ncbi.nlm.nih.gov/pubmed/11106754

Hao, N., Nayak, S., Behar, M., Shanks, R. H., Nagiec, M. J., Errede, B., … Dohlman, H. G. (2008). Regulation of cell signaling dynamics by the protein kinase-scaffold Ste5. *Molecular Cell*, *30*(5), 649–56. http://doi.org/10.1016/j.molcel.2008.04.016

Hartwell, L. H., Mortimer, R. K., Culotti, J., & Culotti, M. (1973). Genetic Control of the Cell Division Cycle in Yeast: V. Genetic Analysis of cdc Mutants. *Genetics*, *74*(2), 267–286.

Hentges, P., Van Driessche, B., Tafforeau, L., Vandenhaute, J., & Carr, A. M. (2005). Three novel antibiotic marker cassettes for gene disruption and marker switching in Schizosaccharomyces pombe. *Yeast*, *22*(13), 1013–1019. http://doi.org/10.1002/yea.1291

Howell, A. S., Jin, M., Wu, C.-F., Zyla, T. R., Elston, T. C., & Lew, D. J. (2012). Negative feedback enhances robustness in the yeast polarity establishment circuit. *Cell*, *149*(2), 322–33. http://doi.org/10.1016/j.cell.2012.03.012

Howell, A. S., Savage, N. S., Johnson, S. a, Bose, I., Wagner, A. W., Zyla, T. R., … Lew, D. J. (2009). Singularity in polarization: rewiring yeast cells to make two buds. *Cell*, *139*(4), 731–743. http://doi.org/10.1016/j.cell.2009.10.024

IBM Corp. (2011). IBM SPSS statistics for Windows, version 20.0. *New York: IBM Corp*. Armonk, NY.

Iden, S., & Collard, J. (2008). Crosstalk between small GTPases and polarity proteins in cell polarization. *Nature Reviews Molecular Cell Biology*. Retrieved from http://www.nature.com/nrm/journal/v9/n11/abs/nrm2521.html

Irazoqui, J. E., Gladfelter, A. S., & Lew, D. J. (2003). Scaffold-mediated symmetry breaking by Cdc42p. *Nature Cell Biology*, *5*(12), 1062–1070. http://doi.org/10.1038/ncb1068

Johnson, J. M., Jin, M., & Lew, D. J. (2011). Symmetry breaking and the establishment of cell polarity in budding yeast. *Current Opinion in Genetics & Development*, *21*(6), 740–746. http://doi.org/10.1016/j.gde.2011.09.007

Justel, A., Pefia, D., & Zamar, R. (1997). A multivariate Kolmogorov-Smimov test of goodness of fit 1, *2*.

Kozubowski, L., Saito, K., Johnson, J. M., Howell, A. S., Zyla, T. R., & Lew, D. J. (2008). Symmetry-breaking polarization driven by a Cdc42p GEF-PAK complex. *Current Biology : CB*, *18*(22), 1719–1726. http://doi.org/10.1016/j.cub.2008.09.060

Krens, S. F. G., Spaink, H. P., & Snaar-Jagalska, B. E. (2006). Functions of the MAPK family in vertebrate-development. *FEBS Letters*, *580*(21), 4984–4990. http://doi.org/10.1016/j.febslet.2006.08.025

Lakhani, V., & Elston, T. C. (2017). Testing the limits of gradient sensing. *PLoS Computational Biology*, *13*(2), 1–30. http://doi.org/10.1371/journal.pcbi.1005386

Landgraf, D., Huh, D., Hallacli, E., & Lindquist, S. (2016). Scarless gene tagging with one-step transformation and two-step selection in Saccharomyces cerevisiae and Schizosaccharomyces pombe. *PLoS ONE*, *11*(10), 1–24. http://doi.org/10.1371/journal.pone.0163950

Layton, A. T., Savage, N. S., Howell, A. S., Carroll, S. Y., Drubin, D. G., & Lew, D. J. (2011). Modeling vesicle traffic reveals unexpected consequences for Cdc42p-mediated polarity establishment. *Current Biology : CB*, *21*(3), 184–194. http://doi.org/10.1016/j.cub.2011.01.012

Lee, M., & Vasioukhin, V. (2008). Cell polarity and cancer--cell and tissue polarity as a non-canonical tumor suppressor. *Journal of Cell Science*, *121*(Pt 8), 1141–50. http://doi.org/10.1242/jcs.016634

Lee, S., Lim, W. A., & Thorn, K. S. (2013). Improved Blue, Green, and Red Fluorescent Protein Tagging Vectors for S. cerevisiae. *PLoS ONE*, *8*(7), 4–11. http://doi.org/10.1371/journal.pone.0067902

Madden, K., & Snyder, M. (1998). Cell polarity and morphogenesis in budding yeast. *Annual Review of Microbiology*, *52*, 687–744. http://doi.org/10.1146/annurev.micro.52.1.687

Marco, E., Wedlich-Soldner, R., Li, R., Altschuler, S., & Wu, L. (2007). Endocytosis optimizes the dynamic localization of membrane proteins that regulate cortical polarity. *Cell*, *129*(2), 411–422. Retrieved from http://www.ncbi.nlm.nih.gov/pmc/articles/PMC2000346/

McClure, A. W., Minakova, M., Dyer, J. M., Zyla, T. R., Elston, T. C., & Lew, D. J. (2015). Role of Polarized G Protein Signaling in Tracking Pheromone Gradients. *Developmental Cell*, *35*(4), 471–482. http://doi.org/10.1016/j.devcel.2015.10.024

Mori, Y., Jilkine, A., & Edelstein-Keshet, L. (2008). Wave-pinning and cell polarity from a bistable reaction-diffusion system. *Biophysical Journal*, *94*(9), 3684–3697. http://doi.org/10.1529/biophysj.107.120824

Narang, A. (2006). Spontaneous polarization in eukaryotic gradient sensing: a mathematical

model based on mutual inhibition of frontness and backness pathways. *Journal of Theoretical Biology*, *240*(4), 538–53. http://doi.org/10.1016/j.jtbi.2005.10.022

Oeztuerk-Winder, F., & Ventura, J.-J. (2012). The many faces of p38 mitogen-activated protein kinase in progenitor/stem cell differentiation. *The Biochemical Journal*, *445*(1), 1–10. http://doi.org/10.1042/BJ20120401

Okada, S., Leda, M., Hanna, J., Savage, N. S., Bi, E., & Goryachev, A. B. (2013). Daughter cell identity emerges from the interplay of Cdc42, septins, and exocytosis. *Developmental Cell*, *26*(2), 148–61. http://doi.org/10.1016/j.devcel.2013.06.015

Onsum, M., & Rao, C. V. (2007). A mathematical model for neutrophil gradient sensing and polarization. *PLoS Computational Biology*, *3*(3), e36. http://doi.org/10.1371/journal.pcbi.0030036

Paliwal, S., Iglesias, P. A., Campbell, K., Hilioti, Z., Groisman, A., & Levchenko, A. (2007). MAPK-mediated bimodal gene expression and adaptive gradient sensing in yeast. *Nature*, *446*(7131), 46–51. http://doi.org/10.1038/nature05561

Raffetto, J. D., Vasquez, R., Goodwin, D. G., & Menzoian, J. O. (2006). Mitogen-activated protein kinase pathway regulates cell proliferation in venous ulcer fibroblasts. *Vascular and Endovascular Surgery*, *40*(1), 59–66. http://doi.org/10.1177/153857440604000108

Rahi, S. J., Larsch, J., Pecani, K., Katsov, A. Y., Mansouri, N., Tsaneva-Atanasova, K., … Cross, F. R. (2017). Oscillatory stimuli differentiate adapting circuit topologies. *Nature Methods*, *14*(10), 1010–1016. http://doi.org/10.1038/nmeth.4408

Reneke, J. E., Blumer, K. J., Courchesne, W. E., & Thorner, J. (1988). The carboxy-terminal segment of the yeast α-factor receptor is a regulatory domain. *Cell*, *55*(2), 221–234. http://doi.org/10.1016/0092-8674(88)90045-1

Richman, T. J., Toenjes, K. a, Morales, S. E., Cole, K. C., Wasserman, B. T., Taylor, C. M., … Johnson, D. I. (2004). Analysis of cell-cycle specific localization of the Rdi1p RhoGDI and the structural determinants required for Cdc42p membrane localization and clustering at sites of polarized growth. *Current Genetics*, *45*(6), 339–49. http://doi.org/10.1007/s00294-004-0505-9

Rikitake, Y., & Liao, J. K. (2005). Rho GTPases, statins, and nitric oxide. *Circulation Research*, *97*(12), 1232–5. http://doi.org/10.1161/01.RES.0000196564.18314.23

Rothstein, R. J. (1983). One-Step Gene Disruption in Yeast. *Methods in Enzymology*, *101*(C), 202–211. http://doi.org/10.1016/0076-6879(83)01015-0

Savage, N. S., Layton, a. T., & Lew, D. J. (2012). Mechanistic mathematical model of polarity in yeast. *Molecular Biology of the Cell*, *23*(10), 1998–2013. http://doi.org/10.1091/mbc.E11-10-0837

Schneider, C. A., Rasband, W. S., & Eliceiri, K. W. (2012). NIH Image to ImageJ: 25 years of image analysis. *Nature Methods*, *9*(7), 671–675. http://doi.org/10.1038/nmeth.2089

Semplice, M., Veglio, a, Naldi, G., Serini, G., & Gamba, a C.-3285628. (2012). A bistable model of cell polarity. *PLoS One*, *7*(2), e30977 ST-A bistable model of cell polarity. http://doi.org/10.1371/journal.pone.0030977

Shapiro, P. (2002). Ras-MAP kinase signaling pathways and control of cell proliferation: relevance to cancer therapy. *Critical Reviews in Clinical Laboratory Sciences*, *39*(4–5), 285–330.

Shinjo, K., Koland, J. G., Hart, M. J., Narasimhan, V., Johnson, D. I., Evans, T., & Cerione, R. a. (1990). Molecular cloning of the gene for the human placental GTP-binding protein Gp (G25K): identification of this GTP-binding protein as the human homolog of the yeast cell-division-cycle protein CDC42. *Proceedings of the National Academy of Sciences of the United States of America*, *87*(24), 9853–7. Retrieved from http://www.pubmedcentral.nih.gov/articlerender.fcgi?artid=55272&tool=pmcentrez&rendertype=abstract

Skupsky, R., Losert, W., & Nossal, R. J. (2005). Distinguishing modes of eukaryotic gradient sensing. *Biophysical Journal*, *89*(4), 2806–23. http://doi.org/10.1529/biophysj.105.061564

Slaughter, B. D., Das, A., Schwartz, J. W., Rubinstein, B., & Li, R. (2009). Dual modes of cdc42 recycling fine-tune polarized morphogenesis. *Developmental Cell*, *17*(6), 823–835. http://doi.org/10.1016/j.devcel.2009.10.022

Smith, G. R., Givan, S. A., Cullen, P., & Sprague, G. F. J. (2002). GTPase-activating proteins for

Cdc42. *Eukaryotic Cell*, *1*(3), 469–480.

Smith, S. E., Rubinstein, B., Mendes Pinto, I., Slaughter, B. D., Unruh, J. R., & Li, R. (2013). Independence of symmetry breaking on Bem1-mediated autocatalytic activation of Cdc42. *The Journal of Cell Biology*, *202*(7), 1091–106. http://doi.org/10.1083/jcb.201304180

Sprague, G. F. J., & Herskowitz, I. (1981). Control of yeast cell type by the mating type locus. I. Identification and control of expression of the a-specific gene BAR1. *Journal of Molecular Biology*, *153*(2), 305–321.

Stevenson, B. J., Ferguson, B., De Virgilio, C., Bi, E., Pringle, J. R., Ammerer, G., & Sprague, G. F. J. (1995). Mutation of RGA1, which encodes a putative GTPase-activating protein for the polarity-establishment protein Cdc42p, activates the pheromone-response pathway in the yeast Saccharomyces cerevisiae. *Genes & Development*, *9*(23), 2949–2963.

Storici, F., & Resnick, M. A. (2006). The Delitto Perfetto Approach to In Vivo Site-Directed Mutagenesis and Chromosome Rearrangements with Synthetic Oligonucleotides in Yeast. *Methods in Enzymology*, *409*(1976), 329–345. http://doi.org/10.1016/S0076-6879(05)09019-1

Subramanian, K. K., & Narang, A. (2004). A mechanistic model for eukaryotic gradient sensing: spontaneous and induced phosphoinositide polarization. *Journal of Theoretical Biology*, *231*(1), 49–67. http://doi.org/10.1016/j.jtbi.2004.05.024

The MathWorks, I. (2015). MATLAB and Statistics Toolbox Release R2015a. Natick, Massachusetts, United States.

Tkach, J. M., Yimit, A., Lee, A. Y., Riffle, M., Costanzo, M., Jaschob, D., … Brown, G. W. (2012). Dissecting DNA damage response pathways by analysing protein localization and abundance changes during DNA replication stress. *Nature Cell Biology*, *14*(9), 966–976. http://doi.org/10.1038/ncb2549

Tong, Z., Gao, X. D., Howell, A. S., Bose, I., Lew, D. J., & Bi, E. (2007). Adjacent positioning of cellular structures enabled by a Cdc42 GTPase-activating protein-mediated zone of inhibition. *Journal of Cell Biology*, *179*(7), 1375–1384. http://doi.org/10.1083/jcb.200705160

Tsygankov, D., Chu, P. H., Chen, H., Elston, T. C., & Hahn, K. M. (2014). User-friendly tools for quantifying the dynamics of cellular morphology and intracellular protein clusters. *Methods in Cell Biology*, *123*, 409–427.

Turing, A. M. (1952). The chemical basis of morphogenesis. *Philosophical Transactions of the Royal Society of London. Series B, Biological Sciences*, *237*(641), 37 LP-72. Retrieved from http://rstb.royalsocietypublishing.org/content/237/641/37.abstract

Tyson, J. J., Chen, K. C., & Novak, B. (2003). Sniffers, buzzers, toggles and blinkers: dynamics of regulatory and signaling pathways in the cell. *Current Opinion in Cell Biology*, *15*(2), 221–231. http://doi.org/10.1016/S0955-0674(03)00017-6

Wai, S. C., Gerber, S. a, & Li, R. (2009). Multisite phosphorylation of the guanine nucleotide exchange factor Cdc24 during yeast cell polarization. *PloS One*, *4*(8), e6563. http://doi.org/10.1371/journal.pone.0006563

Watson, L. J., Rossi, G., & Brennwald, P. (2013). Quantitative Analysis of Membrane Trafficking in Regulation of Cdc42 Polarity, *31*(9), 1713–1723. http://doi.org/10.1109/TMI.2012.2196707.Separate

Wedlich-Soldner, R., Altschuler, S., Wu, L., & Li, R. (2003). Spontaneous cell polarization through actomyosin-based delivery of the Cdc42 GTPase. *Science*, *299*(5610), 1231–1235. Retrieved from http://www.sciencemag.org/content/299/5610/1231.short

Yang, H.-C., & Pon, L. A. (2002). Actin cable dynamics in budding yeast. *Proceedings of the National Academy of Sciences*, *99*(2), 751 LP-756. Retrieved from http://www.pnas.org/content/99/2/751.abstract

Yi, T.-M., Chen, S., Chou, C.-S., & Nie, Q. (2007). Modeling Yeast Cell Polarization Induced by Pheromone Gradients. *Journal of Statistical Physics*, *128*(1–2), 193–207. http://doi.org/10.1007/s10955-007-9285-1

Zhang, W., & Liu, H. T. (2002). MAPK signal pathways in the regulation of cell proliferation in mammalian cells. *Cell Research*, *12*(1), 9–18. http://doi.org/10.1038/sj.cr.7290105

Zheng, Y., Hart, M. J., Shinjo, K., Evans, T., Bender, A., & Cerione, R. A. (1993). Biochemical comparisons of the Saccharomyces cerevisiae Bem2 and Bem3 proteins. Delineation of a

limit Cdc42 GTPase-activating protein domain. *The Journal of Biological Chemistry*, *268*(33), 24629–24634.